Eindhoven University of Technology
Department of Mathematics and Computer Science

Master's Thesis

Progressive Minimum-Link Simplification of Polygonal Curves

by

Wim Reddingius

Supervisor

dr. K.A. Buchin

Eindhoven, July 2017

Abstract

Simplifying polygonal curves at different levels of detail is an important problem with many applications. To facilitate exploration of these simplifications, we wish to seamlessly switch between different levels of detail. These simplifications must thus be consistent with one another. We call such a set of inter-consistent simplifications a *progressive simplification.* Existing geometric optimization algorithms used for curve simplification minimize the complexity of the simplified curve for each level of detail independently. These algorithms therefore do not produce progressive simplifications. All currently known progressive simplification algorithms are based on heuristics and thus do not strictly minimize the simplification complexity.

In this thesis, we wish to bridge the gap between these two types of algorithms. More specifically, we wish to produce progressive simplifications for which the sum or integral of the simplification complexity over all levels of detail is minimized. We present an algorithm that solves this problem in $O(n^3m)$ time, where n is the length of the input curve and m the number of different levels of detail. This algorithm is compatible with any distance measure such as Hausdorff or Fréchet, and can be used to compute an optimal simplification for continuous scaling in $O(n^5)$ time. We further explore two greedy algorithms with a running time of $O(n^2m)$. These algorithms greedily construct each simplification, and may therefore yield a set of simplifications for which the cumulative complexity is non-minimal.

All algorithms proposed in this thesis are based on an existing computational framework that employs finding shortest paths in so-called *shortcut graphs.* These are graphs in which each edge represents a single line segment that is a valid simplification for a contiguous subsequence of the input curve. Each such line segment is called a *shortcut.*

To speed up the simplification algorithms, we present multiple supporting techniques pertaining to these shortcut graphs. First of all, we propose a space-efficient representation of the shortcut graph that can be used to find shortest paths in $O(n \log n)$ time in practice. This is an improvement over using breadth-first search in $O(n^2)$ time. Furthermore, we present an algorithm for efficiently constructing shortcut graphs under the Hausdorff distance for many different levels of detail. This algorithm computes the error of all shortcuts in $O(n^2 \log n)$ time, improving over $O(n^3)$ time using existing techniques.

Experimental evaluation of the developed techniques on animal movement data reveals that the new representation of the shortcut graph drastically lowers the memory usage while significantly improving the running time of using shortcut graphs for curve simplification when compared to existing techniques. The optimal progressive simplification algorithm produces simplifications that are comparable in size to minimal non-progressive simplifications, but was found to be limited to small input curves. We showed that one of the greedy algorithms is a good alternative which produces near-minimal progressive simplifications.

Contents

Chapter 1

Introduction

Given a polygonal curve as input, the *curve simplification* problem asks for a polygonal curve that approximates the input well and that uses as few points as possible. The approximation error between the input curve and the simplification is typically defined by the maximum distance – typically Hausdorff [12] or Fréchet [4] – between an edge of the simplification and the corresponding subcurve of the input. An example of such a simplification is given in Figure 1.1a.

Because of the importance of data reduction, curve simplification has a wide range of applications. Cartography is such an example, where the visual representation of line features such as rivers, roads, countries or boundaries of regions needs to be reduced. Nowadays maps are interactive, so we need curve simplification that works with different levels of detail. Zoomable maps require *progressive simplification*, that is, a simplification that progressively increases the complexity of the representation when zooming in. To illustrate how progressive simplifications are different from non-progressive simplifications, consider Figure 1.1b and Figure 1.1c. Each progressive simplification produces a set of curves that is inter-consistent, meaning if we zoom in on the curve, we add additional detail while retaining the existing points.

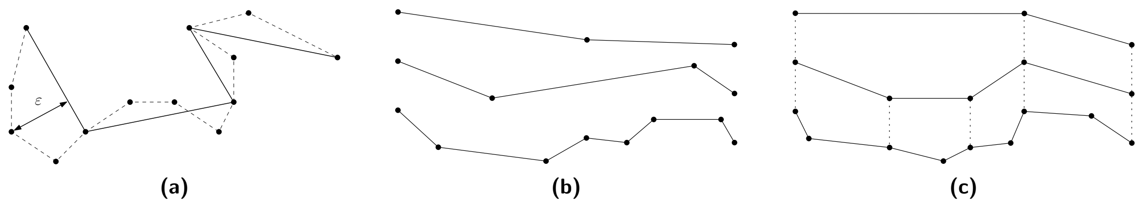

Figure 1.1: (a) Simplification of a polygonal curve from 13 to 5 points, with Hausdorff distance ε. (b) Non-progressive simplification triplet. (c) Progressive simplification triplet.

Existing progressive algorithms (e.g. [5]) work by simplifying a curve, then simplifying the previous simplification, and so on. More concretely, a common approach is to discard the point whose removal introduces the smallest error (according to some criterion). Next, we proceed with a simplification where we remove the point with smallest error from the simplified curve of the previous round. For instance, the algorithm by Visvalingam and Whyatt [24] always removes the point which together with its neighboring points forms the smallest area triangle.

Such approaches stand in stark contrast to (non-progressive) curve simplification algorithms that aim to minimize the complexity of the simplification while guaranteeing a (global) bound on the error between the simplification and the input curve. The most prominent algorithm with a global bound on the Hausdorff distance is the Douglas-Peucker simplification algorithm [10]. While heuristically aiming at a simplification with few points, this algorithm does not actually minimize the number of points. An algorithm that minimizes the number of points and guarantees a certain bound on the simplification error is called a *min-#* simplification. Alternatively, one can fix the number of points in a simplification and minimize its error value ε. This problem is referred to as the *min-ε* simplification problem.

The error bound in existing progressive algorithms is relative to the previous simplification and may accumulate during the simplification process. In this thesis we present the first progressive min-# simplification algorithm which does not compromise the error bound. We extend an existing non-progressive min-# algorithm and are faced with optimizing computational aspects from this algorithm which form a bottleneck either in terms of memory usage or running time. Therefore, we present several supporting techniques for computing min-# simplifications. Although this thesis centers around progressive simplification, these techniques can be applied in a non-progressive setting as well. We further outline these contributions in technical terms at the end of Chapter 2.

Related Work

Curve simplification is a well-studied problem in the past 30 years due to its importance to applications in various domains. Imai and Iri [16] introduced a general approach for computing min-# simplifications by finding shortest paths in so-called *shortcut graphs.* Similar algorithms were presented in a series of papers [17, 23], resulting in algorithms under the Hausdorff distance with a running time of $O(n^2)$ and $O(n^2 \log n)$ for min-# simplification and min-ε simplification respectively [6]. Shortcut graphs are flexible and can be used in conjunction with any error measure. One such error measure was proposed by Imai and Iri [15] for covering rectangles. They solved the min-ε problem for this error measure using an $O(mn(\log n)^2)$-time algorithm minimizing the widths of m covering rectangles.

For the L_1-metric, Agarwal and Varadarajan [2] presented an $O(n^{4/3+\varepsilon})$-time algorithm using a clique-cover to represent the shortcut graph. Agarwal et al. [1] later devised a greedy approximation algorithm for the min-# problem under the Fréchet distance, running in $O(n \log n)$ time. This algorithm produces simplifications for error bound ε that are at most as large as optimal min-# simplifications for error bound $\varepsilon/2$.

Instead of approximation, applications often use heuristics, such as the simplification algorithm by Douglas and Peucker [10]. This algorithm uses the Hausdorff distance, and aims to heuristically minimize the number of points. The worst case running time of this heuristic is $O(n^2)$. Hershberger and Snoeyink [13] showed that this heuristic can be implemented to run in $O(n \log n)$ time, which they later improved to $O(n \log^* n)$ time for non self-intersecting polygonal paths in the *line model* [14].

As previously mentioned, progressive simplifications are commonly used in cartography [19]. A popular such algorithm was proposed by Visvalingam and Whyatt [24], which iteratively removes the point which is part of the triangle with the smallest area. Inspired by this, Daneshpajouh et al. [8] defined an error measure for non-progressive simplification by measuring the sum or the difference in area between a simplification and the input curve. Under the area difference measure, they devised a quadratic-time min-# approximation algorithm.

Chapter 2

Preliminaries

Before delving into the engineering of the algorithms, we present technical details that lie at the core of the problems that we are trying to solve, and the framework we use to solve these problems. The details discussed here will remain central throughout this thesis, and should therefore provide a frame of reference for the chapters to follow.

We open this chapter with a discussion of minimum-link polygonal curve simplifications on a single scale (Section 2.1), followed by how this problem can be extended to produce so-called *progressive simplifications* (Section 2.2). In Section 2.3, we present an existing computational framework used for single-scale simplification which we extend to compute these progressive simplifications. Finally, in Section 2.4 we outline how aspects of this framework relate to the main contributions of this thesis.

2.1 Minimum-link Simplification

In this thesis we are interested in the so called *min-#* problem, which is an optimization problem that takes as input a polygonal curve $\mathcal{C} = \langle p_1, \ldots, p_n \rangle$ represented by a sequence of points in $\mathbb{R}^d$ where $d > 1$, and an error bound $\varepsilon \geq 0$. We wish to simplify this polygonal curve to a polygonal curve $\mathcal{S}$ on which the following conditions hold:

- The size of $\mathcal{S}$ should be minimized, meaning $|\mathcal{S}|$ is minimal.
- $\mathcal{S}$ sufficiently approximates $\mathcal{C}$, meaning $\mathcal{D}(\mathcal{C}, \mathcal{S}) \leq \varepsilon$, where $\mathcal{D}$ is an error function.

Different error functions $\mathcal{D}$ exist that define how the similarity, or "distance", between polygonal curves is determined or measured. Among these error functions are the *Hausdorff distance* [12], and the *Fréchet distance* [4]. In this thesis, we will mostly consider the Hausdorff distance. However, most of these error measures are computed with the same time complexity, meaning that in many cases any error measure can be used. To define the Hausdorff distance, we use $p \dashv P$ to denote *any* point p that lies on polygonal curve P.

Hausdorff Distance: *For any two polygonal curves P and Q, the Hausdorff distance $\mathcal{H}(P, Q)$ is defined as:*

$$\mathcal{H}(P,Q) = \max[\mathcal{H}(P \to Q), \mathcal{H}(Q \to P)]$$
$$\mathcal{H}(P \to Q) = \max_{p \dashv P} \min_{q \dashv Q} \; dist(p,q)$$

We use $dist(x, y)$ to denote the Euclidean distance between points x and y.

Simply stated, the Hausdorff distance is the greatest of all the distances from a point on one of the curves to the closest point on the other curve. These distances are visualized in Figure 2.1a and Figure 2.1b. By limiting this distance to ε, all points of the simplification $\mathcal{S}$ must remain within the *tolerance region* of $\mathcal{C}$. This is visualized for a single line segment in Figure 2.1c.

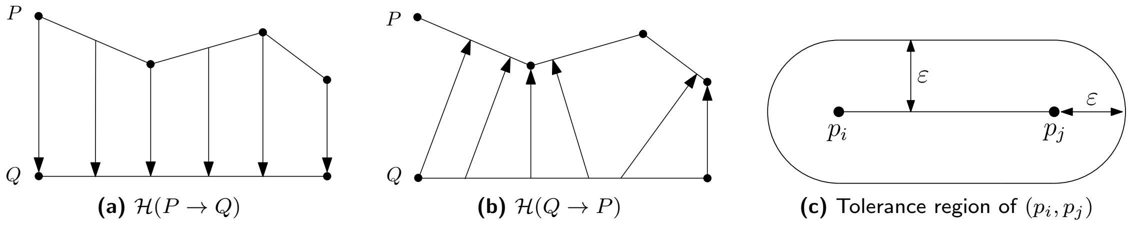

(a) $\mathcal{H}(P \to Q)$ **(b)** $\mathcal{H}(Q \to P)$ **(c)** Tolerance region of (p_i, p_j)

Figure 2.1: The Hausdorff distance.

Note how the problem as defined so far has a solution set which is continuous, since points of $\mathcal{S}$ may be chosen anywhere in $\mathbb{R}^d$. The min-# problem is therefore typically simplified such that $\mathcal{S}$ is a subsequence of $\mathcal{C}$ including p_1 and p_n. This has the advantage that there is a clear association between segments of $\mathcal{S}$ and subcurves of $\mathcal{C}$. Therefore, if $\mathcal{S}$ contains the line segment (p_i, p_j), we want the subcurve of $\mathcal{C}$ from p_i to p_j to be close to this segment. This gives us the following set of constraints:

- $\mathcal{S}$ is a subsequence of $\mathcal{C}$, denoted $\mathcal{S} \sqsubseteq \mathcal{C}$.
- The first and last point of $\mathcal{C}$ must be part of any simplification, thus $p_1, p_n \in \mathcal{S}$.
- Any line segment $(p_i, p_j) \in \mathcal{S}$ sufficiently approximates the subsequence $\langle p_i, \dots, p_j \rangle \sqsubseteq \mathcal{C}$. We therefore have $\max_{(p_i,p_j)\in\mathcal{S}} \mathcal{D}(\langle p_i, \dots, p_j \rangle, \langle p_i, p_j \rangle) \leq \varepsilon$.

By redefining the error this way, we are more stringent on the shape of simplification $\mathcal{S}$ with respect to the input curve $\mathcal{C}$. For instance, by defining the Hausdorff distance globally, i.e. $\mathcal{H}(\mathcal{C}, \mathcal{S}) \leq \varepsilon$, the closest point on $\mathcal{C}$ to any point on $\mathcal{S}$ can be picked anywhere on $\mathcal{C}$, and vice versa. Therefore, some edges of $\mathcal{S}$ may poorly approximate the corresponding subsequence on $\mathcal{C}$, without violating the maximum Hausdorff distance. This is illustrated in Figure 2.2.

This definition of the error on subsequences of $\mathcal{C}$ also facilitates area-based error measures, such as the measures suggested by Daneshpajouh et al. [8]. These measures define the error of line segment $(p_i, p_j) \in \mathcal{S}$ in terms of the area of the simple polygons formed by the intersections of $\langle p_i, p_j \rangle$ and $\langle p_i, \dots, p_j \rangle$.

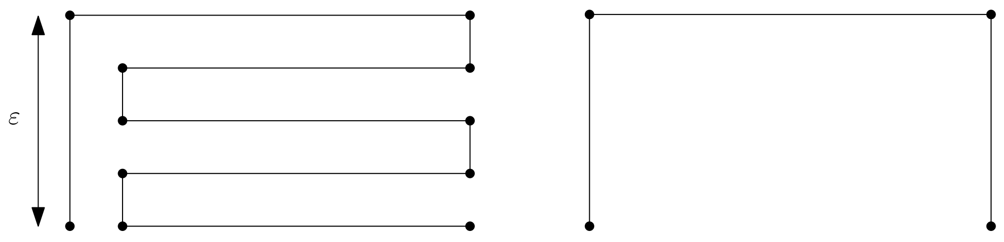

(a) Polygonal curve $\mathcal{C}$ **(b)** Simplification $\mathcal{S} \sqsubseteq \mathcal{C}$

Figure 2.2: An example where globally defining the Hausdorff distance gives a simplification where the shape of $\mathcal{C}$ is lost. Note that $\mathcal{H}(\mathcal{C}, \mathcal{S}) \leq \varepsilon$, but $\max_{(p_i,p_j)\in\mathcal{S}} \mathcal{H}(\langle p_i, \dots, p_j \rangle, \langle p_i, p_j \rangle) > \varepsilon$.

Another advantage of imposing a maximum error on each subsequence, is that most error measures are considerably easier to compute when one of the polygonal curves is just a single line

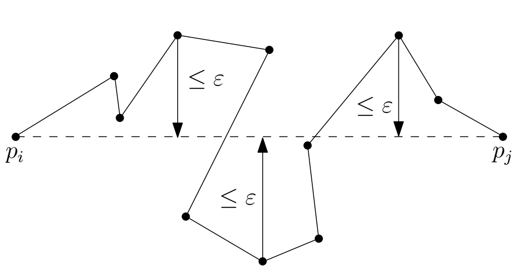

(a) $\max_{p_k \in \langle p_i, \ldots, p_j \rangle} dist(p_k, (p_i, p_j)) \leq \varepsilon$

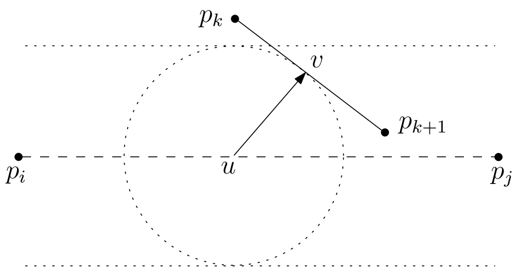

(b) $dist(u, v) > \mathcal{H}(\langle p_i, \ldots, p_j \rangle \rightarrow \langle p_i, p_j \rangle)$

Figure 2.3: Computing the Hausdorff distance between $\langle p_i, p_j \rangle$ and $\langle p_i, \ldots, p_j \rangle$.

segment. For example, we measure the Hausdorff distance between a line segment $(p_i, p_j) \in \mathcal{S}$, and the corresponding contiguous subsequence in $\mathcal{C}$ by measuring the distance from line segment (p_i, p_j) to the furthest point in the subsequence $\langle p_i, \ldots, p_j \rangle$. This is illustrated in Figure 2.3a. We now prove that this indeed computes $\mathcal{H}(\langle p_i, \ldots, p_j \rangle, \langle p_i, p_j \rangle)$. For this, we define $dist(p_k, (p_i, p_j))$ as the length of the line segment perpendicular to (p_i, p_j) which joins p_k to (p_i, p_j). This distance is also called the perpendicular distance from a point to a line.

Lemma 2.1. *For any polygonal curve* $\mathcal{C} = \langle p_1, \ldots, p_n \rangle$, *the Hausdorff distance* $\mathcal{H}(\langle p_i, \ldots, p_j \rangle, \langle p_i, p_j \rangle)$ *of any line segment* (p_i, p_j) *where* $1 \leq i < j \leq n$ *is equal to* $\max_{p_k \in \langle p_i, \ldots, p_j \rangle} dist(p_k, (p_i, p_j))$.

Proof. We know that the shortest distance from a line segment (p_i, p_j) to a point $p_k \dashv \mathcal{C}$ is the same as the shortest distance from (p_i, p_j) to a point $p_k \in \mathcal{C}$. This means we have:

$$\begin{aligned} & \mathcal{H}(\langle p_i, \ldots, p_j \rangle \rightarrow \langle p_i, p_j \rangle) \\ = & \max_{x \dashv \langle p_i, \ldots, p_j \rangle} \min_{y \dashv (p_i, p_j)} dist(x, y) \\ = & \max_{p_k \in \langle p_i, \ldots, p_j \rangle} \min_{y \dashv (p_i, p_j)} dist(p_k, y) \\ = & \max_{p_k \in \langle p_i, \ldots, p_j \rangle} dist(p_k, (p_i, p_j)) \end{aligned}$$

Now let us assume that $\mathcal{H}(\langle p_i, p_j \rangle \rightarrow \langle p_i, \ldots, p_j \rangle) > \mathcal{H}(\langle p_i, \ldots, p_j \rangle \rightarrow \langle p_i, p_j \rangle)$. This means that there is a point $u \dashv (p_i, p_j)$ for which there is a closest point v on some line segment (p_k, p_{k+1}) in the subsequence $\langle p_i, \ldots, p_j \rangle$, such that the distance between u and v is larger than $\mathcal{H}(\langle p_i, \ldots, p_j \rangle \rightarrow \langle p_i, p_j \rangle)$. This situation is sketched in Figure 2.3b. Note that $\langle p_i, \ldots, p_j \rangle$ cannot pass through the illustrated circle with radius $dist(u, v)$, since otherwise v is not the closest point from u on $\langle p_i, \ldots, p_j \rangle$. Furthermore, $\langle p_i, \ldots, p_j \rangle$ cannot touch or cross the boundaries sketched at the top and the bottom, because otherwise $\mathcal{H}(\langle p_i, \ldots, p_j \rangle \rightarrow \langle p_i, p_j \rangle) \geq dist(u, v) > \mathcal{H}(\langle p_i, \ldots, p_j \rangle \rightarrow \langle p_i, p_j \rangle)$. Therefore, there is no conceivable configuration of $\langle p_i, \ldots, p_j \rangle$. By contradiction, we may thus conclude $\mathcal{H}(\langle p_i, p_j \rangle \rightarrow \langle p_i, \ldots, p_j \rangle) \leq \mathcal{H}(\langle p_i, \ldots, p_j \rangle \rightarrow \langle p_i, p_j \rangle)$.

Using the definition of the Hausdorff distance, we conclude $\mathcal{H}(\langle p_i, \ldots, p_j \rangle, \langle p_i, p_j \rangle)$ is equal to $\max_{p_k \in \langle p_i, \ldots, p_j \rangle} dist(p_k, (p_i, p_j))$. □

Although the min-# problem is well defined for any number of dimensions, we will solely focus on two-dimensional polygonal curves. We can now formally define the problem as follows:

Single Scale Min-#
Input: A polygonal curve $\mathcal{C} = \langle p_1, \ldots, p_n \rangle$ in $\mathbb{R}^2$, and an error bound $\varepsilon \geq 0$.
Output: A polygonal curve $\mathcal{S}$ in $\mathbb{R}^2$ where $\mathcal{S} \sqsubseteq \mathcal{C}$, such that $|\mathcal{S}|$ is minimal, and:

- $p_1 \in \mathcal{S}$ and $p_n \in \mathcal{S}$.
- $\max_{(p_i, p_j) \in \mathcal{S}} \mathcal{D}(\langle p_i, \ldots, p_j \rangle, \langle p_i, p_j \rangle) \leq \varepsilon$.

2.2 Progressive Simplification

By extending the min-# simplification problem to multiple scales, we are concerned with finding m simplifications $\langle \mathcal{S}_1, \dots, \mathcal{S}_m \rangle$ for m error bounds $\mathcal{E} = \langle \varepsilon_1, \dots, \varepsilon_m \rangle$ where $\varepsilon_m > \dots > \varepsilon_1 \geq 0$.

We can construct each simplification $\mathcal{S}_k$ by using any algorithm to solve Single Scale Min-# for $\mathcal{C}$ and ε_k. However, by constructing each simplification independently, we run the risk that some simplifications have a different shape than others. To facilitate interactive exploration of these simplifications where one can seamlessly switch between different simplifications, we therefore desire some form of inter-consistency. More specifically, we require a mapping from each subsequence of points in $\mathcal{S}_i$ to a subsequence of points in $\mathcal{S}_j$ where $i \neq j$. The points shared between any two simplifications thereby provide a frame of reference by which one can infer the relationship between these simplifications.

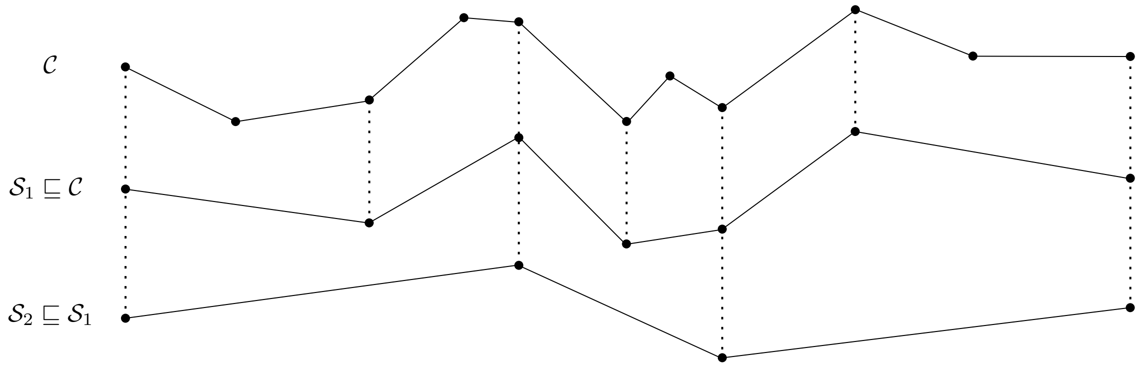
$\mathcal{C}$
$\mathcal{S}_1 \sqsubseteq \mathcal{C}$
$\mathcal{S}_2 \sqsubseteq \mathcal{S}_1$

Figure 2.4: Mapping of subsequences of $\mathcal{C}$ across progressive simplifications.

We perform this mapping by enforcing *monotonic containment* on the points of each simplification, from $\mathcal{S}_m$ to $\mathcal{S}_1$. We thus require $\mathcal{S}_i \sqsubseteq \mathcal{S}_{i-1}$ for all $1 < i \leq m$, and $\mathcal{S}_1 \sqsubseteq \mathcal{C}$. This way, detail is progressively added to simplifications at lower scales. Figure 2.4 illustrates this monotonic containment relation. We call each set of simplifications of $\mathcal{C}$ for $\mathcal{E}$ that adheres to this monotonic containment relation a *progressive simplification*. The min-# progressive simplification problem can be defined as follows:

Progressive Min-#
Input: A polygonal curve $\mathcal{C} = \langle p_1, \dots, p_n \rangle$ in $\mathbb{R}^2$ and a sequence of error bounds $\mathcal{E} = \langle \varepsilon_1, \dots, \varepsilon_m \rangle$ where $\varepsilon_m > \dots > \varepsilon_1 \geq 0$.
Output: A sequence of polygonal curves $\langle \mathcal{S}_1, \dots, \mathcal{S}_m \rangle$ in $\mathbb{R}^2$ where $\mathcal{S}_m \sqsubseteq \dots \sqsubseteq \mathcal{S}_1 \sqsubseteq \mathcal{C}$, such that $\sum_{i=1}^{m} |\mathcal{S}_i|$ is minimal, and for all $1 \leq i \leq m$ we have:

- $p_1 \in \mathcal{S}_i$, and $p_n \in \mathcal{S}_i$.
- $\max_{(p_x,p_y) \in \mathcal{S}_i} \mathcal{D}(\langle p_x, \dots, p_y \rangle, \langle p_x, p_y \rangle) \leq \varepsilon_i$.

If we wish to prioritize the minimization of simplifications at specific scales, we can generalize Progressive Min-# such that we have a weight for every simplification which represents the importance of the minimization of that simplification. We thus have a sequence of weights $\mathcal{W} = \langle w_1, \dots, w_m \rangle$ in $\mathbb{R}$, where $w_i > 0$ for all $1 \leq i \leq m$. We now wish to minimize $\sum_{i=1}^{m} w_i |\mathcal{S}_i|$. We call this generalized problem Weighted Progressive Min-#.

So far we have considered discrete progressive simplifications, meaning we simplify for a given set of error bounds. We may instead want to simplify continuously, capturing every possible level of detail. We thus wish to find a simplification $\mathcal{S}_\varepsilon$ for all $0 \leq \varepsilon \leq \varepsilon_z$, where $\varepsilon_z = \mathcal{D}(\langle p_1, \dots, p_n \rangle, \langle p_1, p_n \rangle)$, which is the error of simplification $\langle p_1, p_n \rangle$. Note that monotonic containment is still imposed, implying $\mathcal{S}_{\varepsilon'} \sqsubseteq \mathcal{S}_\varepsilon$ for all $\varepsilon' > \varepsilon$. The goal is to minimize the cumulative size of this continuous set of simplifications. We thus want to minimize $\int_0^{\varepsilon_z} |\mathcal{S}_\varepsilon|\, d\varepsilon$. We call this continuous generalization Continuous Progressive Min-#. Now let us prove that Continuous Progressive Min-# can be reduced to Weighted Progressive Min-#.

Lemma 2.2. *Given a polygonal curve $\mathcal{C} = \langle p_1, \ldots, p_n \rangle$, we can solve* Continuous Progressive Min-# *by solving* Weighted Progressive Min-# *for $\binom{n}{2}$ error bounds.*

Proof. Assume we have the error $\mathcal{D}(\langle p_i, \ldots, p_j \rangle, \langle p_i, p_j \rangle)$ of every line segment (p_i, p_j) where $j > i$. Let $\langle \varepsilon_1, \ldots \varepsilon_{\binom{n}{2}} \rangle$ be the sorted list of these errors in ascending order without duplicates. Note that it is possible that $\varepsilon_z < \varepsilon_{\binom{n}{2}}$.

Now consider the claim $\mathcal{S}_\varepsilon = \mathcal{S}_{\varepsilon_i}$ for all $\varepsilon \in [\varepsilon_i, \varepsilon_{i+1})$. We know this holds, since assuming $\mathcal{S}_\varepsilon < \mathcal{S}_{\varepsilon_i}$ would imply all $\mathcal{S}_{\varepsilon'}$ where $\varepsilon' \in [\varepsilon_i, \varepsilon]$ are not minimal. Therefore, we have

$$\int_0^{\varepsilon_z} |\mathcal{S}_\varepsilon|\, d\varepsilon = \sum_{k=1}^{z-1} (\varepsilon_{k+1} - \varepsilon_k) |\mathcal{S}_{\varepsilon_k}|$$

Thus, we can solve Continuous Progressive Min-# by solving Weighted Progressive Min-# for error bounds $\mathcal{E} = \langle \varepsilon_1, \ldots \varepsilon_z \rangle$ and weights $\mathcal{W} = \langle w_1, \ldots, w_z \rangle$, where $w_i = \varepsilon_{i+1} - \varepsilon_i$ for all $1 \leq i < z$.

2.3 Computational Framework

In order to solve the problems stated in the previous sections, we use a computational framework proposed by Imai and Iri [16]. This framework uses the notion of a *shortcut*, which is defined as follows:

Shortcut: *For any polygonal curve $\mathcal{C} = \langle p_1, \ldots, p_n \rangle$ and an error bound $\varepsilon \geq 0$, any line segment (p_i, p_j) where $j > i$ is a shortcut of $\mathcal{C}$ for ε if and only if $\mathcal{D}(\langle p_i, \ldots, p_j \rangle, \langle p_i, p_j \rangle) \leq \varepsilon$.*

Intuitively, a shortcut (p_i, p_j) is a line segment that sufficiently approximates all points in $\mathcal{C}$ between p_i and p_j, given an error bound ε. Hence, a shortcut of $\mathcal{C}$ for ε is a line segment that can be included in any simplification $\mathcal{S}$ with an error bound of at most ε. Note how for any $1 \leq i < m$, (p_i, p_{i+1}) is always a shortcut, regardless of $\mathcal{C}$ and ε, because we always have $\mathcal{D}(\langle p_i, p_j \rangle, \langle p_i, p_j \rangle) = 0$.

The computational framework defines a *shortcut graph* as a graph that contains all shortcuts for a given error bound as its edges. We formally define this graph as follows:

Shortcut Graph: *Given a polygonal curve $\mathcal{C} = \langle p_1, \ldots, p_n \rangle$ and an error bound $\varepsilon \geq 0$, a shortcut graph is a graph $G(\mathcal{C}, \varepsilon) = (V, E)$, where $V = \mathcal{C}$ and $E = \{\ (p_i, p_j) \mid (p_i, p_j)$ is a shortcut of $\mathcal{C}$ for $\varepsilon\ \}$.*

We can solve Single Scale Min-# by finding a shortest path from p_1 to p_n in $G(\mathcal{C}, \varepsilon)$ using a breadth-first search [18] in $O(n^2)$ time. An example of each step of the computational framework is shown in Figure 2.5.

To prove correctness of this framework, we first show that any simplification it creates is valid, meaning that each of its edges adheres to the error bound. We furthermore prove that it is minimal by showing that there cannot be another valid simplification that is smaller.

Lemma 2.3. *For any polygonal curve $\mathcal{C} = \langle p_1, \ldots, p_n \rangle$ and an error bound $\varepsilon \geq 0$, if π is a path in $G(\mathcal{C}, \varepsilon)$, then $\max_{(p_i,p_j) \in \pi} \mathcal{D}(\langle p_i, \ldots, p_j \rangle, \langle p_i, p_j \rangle) \leq \varepsilon$.*

Proof. For any $(p_i, p_j) \in \pi$, we know $\mathcal{D}((p_i, \ldots, p_j), \langle p_i, p_j \rangle) \leq \varepsilon$, since $(p_i, p_j) \in G(\mathcal{C}, \varepsilon)$. Since (p_i, p_j) is an arbitrary edge in π, we conclude $\max_{(p_i,p_j) \in \pi} \mathcal{D}(\langle p_i, \ldots, p_j \rangle, \langle p_i, p_j \rangle) \leq \varepsilon$. □

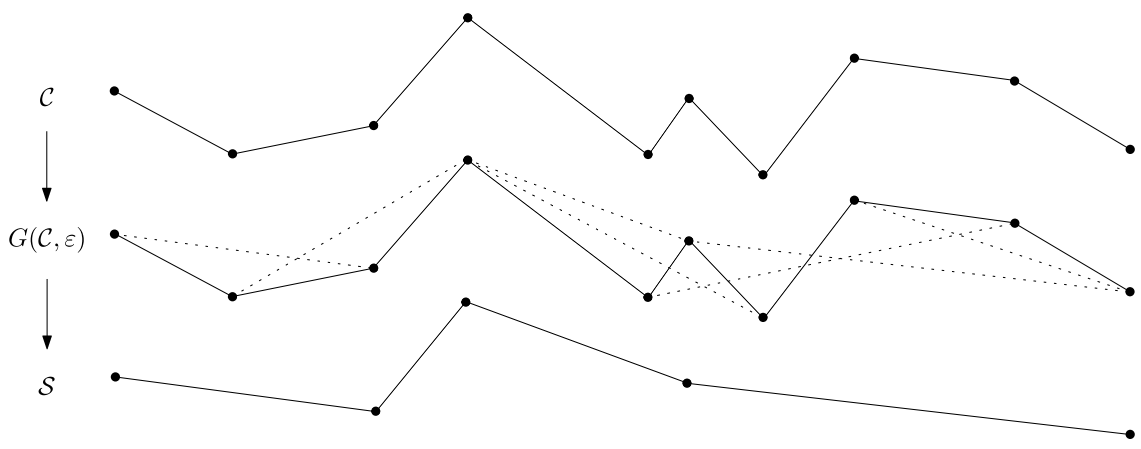

Figure 2.5: Simplification by finding shortest paths in shortcut graphs.

Lemma 2.4. *For any polygonal curve $\mathcal{C} = \langle p_1, \ldots, p_n \rangle$ and an error bound $\varepsilon \geq 0$, any shortest path π from p_1 to p_n in $G(\mathcal{C}, \varepsilon)$ is at most as long as any smallest polygonal curve $\mathcal{S}$ for which $\max_{(p_i,p_j) \in \mathcal{S}} \mathcal{D}(\langle p_i, \ldots, p_j \rangle, \langle p_i, p_j \rangle) \leq \varepsilon$, $\mathcal{S} \sqsubseteq \mathcal{C}$ and $p_1, p_n \in \mathcal{S}$.*

Proof. Consider any edge $(p_i, p_j) \in \mathcal{S}$. For this edge we have $\mathcal{D}((p_i, \ldots, p_j), \langle p_i, p_j \rangle) \leq \varepsilon$. Therefore, (p_i, p_j) must be a shortcut of $\mathcal{C}$ for ε which means that (p_i, p_j) is an edge in $G(\mathcal{C}, \varepsilon)$. Because (p_i, p_j) is an arbitrary link in $\mathcal{S}$, the polygonal curve $\mathcal{S}$ must be a path in $G(\mathcal{C}, \varepsilon)$. Because π is a shortest path from p_1 to p_n in $G(\mathcal{C}, \varepsilon)$, we conclude $|\pi| \leq |\mathcal{S}|$. □

2.4 Contributions

Throughout this thesis we discuss different adaptions of the computational framework described in Section 2.3. In Chapter 3, we investigate an alternative representation of the shortcut graph called a *shortcut interval set*. In practice, this representation has sub-quadratic storage requirements which allows us to find shortest paths in $O(n \log n)$ time. This is an improvement over using breadth-first search in an explicit representation of the shortcut graph using $O(n^2)$ time and space. Experimental evaluation reveals that a significant improvement is realized by using shortcut interval sets, both in terms of memory usage and running time.

In Chapter 4, we discuss how shortcut graphs can efficiently be constructed for many different error bounds using the Hausdorff distance. We present an algorithm that computes for each line segment the maximum error at which it is a valid shortcut. These errors can be used to efficiently construct the shortcut graph associated with any error bound. This algorithms runs in $O(n^2 \log n)$ time, which is an improvement over $O(n^3)$ time using existing techniques by Imai and Iri [16]. The results indicate that this algorithm yields benefits over existing techniques, but only when constructing a large number of shortcut graphs. This algorithm is therefore only suitable when simplifying for many different levels of detail.

Finally, In Chapter 5 we elaborate on how we can use shortcut graphs to compute progressive simplifications. We present the first progressive min-# simplifications algorithm running in $O(n^3 m)$ time. We furthermore propose two $O(n^2 m)$-time greedy algorithms which do not strictly minimize the cumulative simplification size. Analysis of the performance of these algorithms in practice reveals that the optimal progressive simplification algorithm produces simplifications that are comparable in size to minimal non-progressive simplifications. However, we found that this algorithm is unscalable to large input curves due to its cubic time complexity. One of the greedy algorithms was shown to be a good alternative which produces near-minimal progressive simplifications.

Chapter 3

Exploiting Real-World Structures in the Shortcut Graph

As outlined in Section 2.3, the data structure central to the computational framework is the shortcut graph. This graph encodes all contiguous subsequences of $\mathcal{C}$ which can be sufficiently approximated with a single line segment called a shortcut. A natural way of implementing a graph is by storing all edges incident to any node explicitly. We refer to shortcut graphs that are implemented this way as *explicit shortcut graphs.* In this chapter, we present how common patterns in real-world data can be exploited to obtain a compressed representation of the shortcut graph, called a *shortcut interval set.* Aside from lowering memory usage, this representation aims to optimize running time of finding shortest paths in practice.

We open this chapter with an outline of the aforementioned patterns and how they can be used to compress the shortcut graph to a sub-quadratic representation (Section 3.1). Next, we address how this new representation can be integrated with the computational framework to find shortest paths (Section 3.2). Finally, we experimentally evaluate how effective the compression of this new representation is in practice (Section 3.3).

3.1 Shortcut Intervals

As outlined in Chapter 1, polygonal curve simplification is mostly applied to spatial data, such as line features on a map, or movement trajectories of migratory animals. Most types of spatial data are structured, and follow the following common intuitions:

- Most consecutive points are near one another.
- Most consecutive line segments have similar heading.

Whenever these patterns are present, we expect most consecutive points p_i and p_j to share points with which they form shortcuts. This means that when (p_x, p_i) is a shortcut for some point p_x, we expect (p_x, p_j) to be a shortcut as well. Similarly, if (p_i, p_y) is a shortcut for some point p_y, we expect (p_j, p_y) to be a shortcut. This yields contiguous subsequences of $\mathcal{C}$ with which p_i forms a sequence of shortcuts. This is illustrated in Figure 3.1. We call each such subsequence a *shortcut interval*, which is defined as follows:

Shortcut Interval: *For any polygonal curve $\mathcal{C} = \langle p_1, \dots, p_n \rangle$, an error bound $\varepsilon \geq 0$, and $1 \leq i < x \leq y \leq n$, the interval $[x, y]$ is a shortcut interval for p_i and ε if and only if for all $x \leq z \leq y$, (p_i, p_z) is a shortcut of $\mathcal{C}$ for ε, and $[x, y]$ is maximal.*

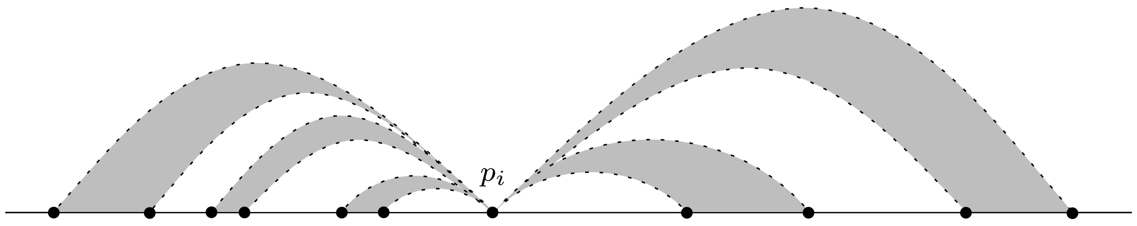

Figure 3.1: Shortcut intervals associated with some point p_i.

We combine these shortcuts intervals into sets called *shortcut interval sets*, which are defined as follows:

Shortcut Interval Set: *For any polygonal curve $\mathcal{C} = \langle p_1, \ldots, p_n \rangle$ and an error bound $\varepsilon \geq 0$, a shortcut interval set of $\mathcal{C}$ for ε is a set $I(\mathcal{C}, \varepsilon) = \langle I_1(\varepsilon), \ldots, I_n(\varepsilon) \rangle$ where for all $1 \leq i \leq n$, $I_i(\varepsilon)$ is the collection of all shortcut intervals $[x, y]$ for p_i and ε.*

Note that a shortcut interval set is a minimally sized set of shortcut intervals that covers all shortcuts. We can visualize a shortcut interval set in a matrix where the rows and columns correspond to the points in $\mathcal{C}$, and the shading of each cell at position i, j corresponds to whether (p_i, p_j) is a shortcut. In Figure 3.2, we can see such matrices for four different error bounds. Note how regardless of the error bound, every row and column only has a few black regions. This means we typically have $|I_i| = O(1)$ shortcut intervals for any $p_i \in \mathcal{C}$. This implies that $I(\mathcal{C}, \varepsilon)$ has a storage complexity of $O(n)$ in practice, regardless of ε. This is an order of magnitude smaller than the explicit representation of the shortcut graph $G(\mathcal{C}, \varepsilon)$, which has a storage complexity of $O(n^2)$.

Similar compression techniques were used by Alewijnse et al. [3] to speed up trajectory segmentation.

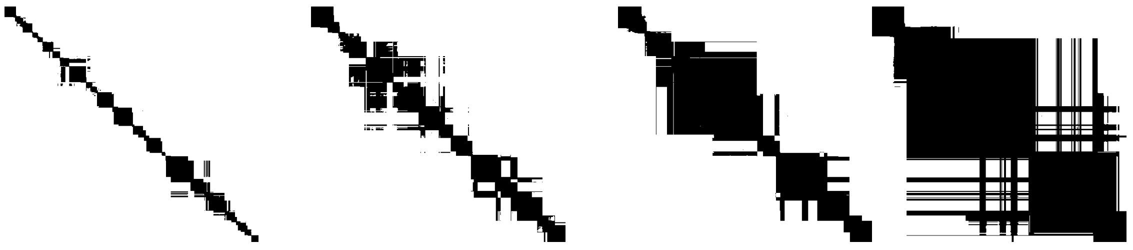

Figure 3.2: Matrix visualization of the shortcut interval sets of a polygonal curve composed of 757 points for four different error bounds. Each black cell represents a shortcut.

3.2 Finding Shortest Paths

Let us now discuss how we can find shortest paths from a source node p_s to a target node p_t in a shortcut interval set. On explicit shortcut graphs, this is most efficiently computed using breadth-first search in $O(n^2)$ time [18]. In this section we elaborate on how we can exploit shortcut intervals to improve this running time in practice.

We construct a balanced binary search tree T containing every point $p_i \in \langle p_s, \ldots, p_t \rangle$ ordered by the index i of any point p_i. Consider we have a point $p_b \in T$ where all points in $\langle p_a, \ldots, p_c \rangle$ are rooted at p_b. We wish to annotate p_b with the following two paths:

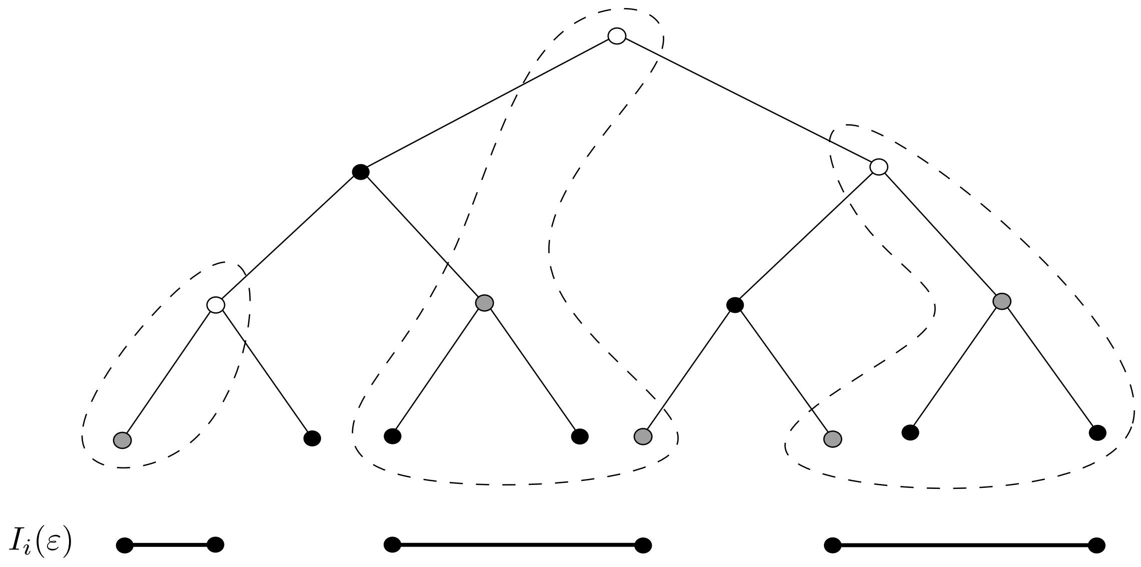

Figure 3.3: Finding the shortest path from p_i to p_t by means of range queries. For every grey node we consider the subtree annotation, and for every white node we consider the node annotation.

- A shortest path from p_b to p_t.
- A shortest path from any point in $\langle p_a, \dots, p_c \rangle$ to p_t.

We therefore have an annotation of every node, and of every subtree. We represent the subtree annotation using the path's *first* point (some point in $\langle p_a, \dots, p_c \rangle$) and the path's length. The node annotation is represented using the path's *second* point (the point after p_b) and the path's length. This way, the annotations encode the next step in a shortest path to p_t. Any shortest path can therefore be reconstructed by following the annotations from node to node until we reach p_t.

The complete annotation of T is achieved by inserting every point p_i in $\mathcal{C}$ from p_t down to p_s in sequence, and obtaining the node annotation of p_i using a customized range query on the binary search tree for every shortcut interval in $I_i(\varepsilon)$. Every range query for shortcut interval $[x, y] \in I_i(\varepsilon)$ finds shortest path candidates from p_j to p_t where (p_i, p_j) is a shortcut of $\mathcal{C}$ for ε and $x \le j \le y$. Specifically, we start at the root node of T, and for every node p_b where all nodes in $\langle p_a, \dots, p_c \rangle$ are rooted at p_b, we do the following:

- If $x \le a \le c \le y$, consider the subtree annotation of p_b.
- Otherwise:
  - If $x \le b \le y$, consider the node annotation of p_b.
  - If $x < b$ and $y \ge a$, traverse to the left child of p_b, containing points p_i where $i < b$.
  - If $y > b$ and $x \le c$, traverse to the right child of p_b, containing points p_i where $i > b$.

In the first case we have $x \le a \le c \le y$, and therefore all points in $\langle p_a, \dots, p_c \rangle$ lie in the shortcut interval $[x, y]$, meaning that the subtree annotation of p_b is a path that can be prepended with p_i to form a path from p_i to p_t. By performing these range queries, we therefore efficiently collect the shortest possible paths from p_i to p_t via all shortcuts in $I_i(\varepsilon)$. An example is given in Figure 3.3.

After all candidate paths are found, we choose the path π with the shortest length. We prepend π with p_i, and use this path as the node annotation of p_i. The subtree annotation of p_i is efficiently maintained using the node annotation of p_i and the subtree annotation of both children of p_i.

After all points are inserted, we reconstruct the shortest path from p_s to p_t using the node annotation of p_s.

Running time Each range query on some shortcut interval $[x, y]$ follows a path down the search tree T to locate a subtree which has p_x as a minimum. Similarly, we locate a subtree which has p_y as a maximum. We therefore only traverse the children of at most two nodes at any level of the binary search tree. This means that on each level of the tree, we spend $O(1)$ time. Since the binary search tree is balanced, it has a height of $O(\log n)$. Each range query therefore takes $O(\log n)$ time.

Furthermore, note that annotating the tree does not influence the asymptotic running time of inserting a node. This is because any subtree annotation of some node only has a possible impact on the subtree annotation of all its ancestors. The subtree annotation of a node is maintained in $O(1)$ by checking the subtree annotation of both its children. Because the tree is balanced, any node has at most $O(\log n)$ ancestors, implying that updating these annotations takes at most $O(\log n)$ time.

We conclude that each range query and insertion takes $O(\log n)$ time in the worst case. We know that for all $s \leq i \leq t$, we typically have $|I_i(\varepsilon)| = O(1)$, and we therefore perform $O(1)$ range queries for every point in practice. Since we may need to insert $O(n)$ points, finding a shortest path in a shortcut interval set therefore takes $O(n \log n)$ time in practice. In the worst case, we have $O(n^2)$ shortcut intervals in total, in which case the running time is $O(n^2 \log n)$.

Optimization Despite the expectation that $|I_i(\varepsilon)| = O(1)$ for any point p_i, it is possible that some shortcut intervals in $I_i(\varepsilon)$ are infinitesimal. In the worst case, a shortcut interval is so small that performing the range query takes more time than simply checking the node annotation of all points in the interval. Therefore, if a shortcut interval $[x, y] \in I_i(\varepsilon)$ is smaller than $O(\log n)$, we can save time by doing a brute force determination of the corresponding shortest path in $O(y - x)$ time.

Note how this influences the worst case number of range queries from $O(n)$ to $O(\frac{n}{\log n})$. Because each range query takes $O(\log n)$ time, we conclude that this optimization brings the worst case running time down to $O(n^2)$.

3.3 Experimental Evaluation

The performance of using shortcut interval sets to find shortest paths depends highly on the signature of $\mathcal{C}$, and the signature of the shortcut intervals contained in $I(\mathcal{C}, \varepsilon)$. In this section we therefore investigate both the impact of using shortcut interval sets for a variable length of input curve $\mathcal{C}$, and for a variable error bound ε.

One motivation for progressively simplifying polygonal curves is to visualize and interactively explore movement trajectories on multiple scales. All algorithms and techniques presented in this thesis are therefore experimentally evaluated using a movement trajectory. More specifically, we use a movement trajectory of a griffon vulture migrating across south Europe by Shmidt-Rothmund [21]. This trajectory is shown on a geographic map in Figure 3.4. This is a trajectory composed of 340.000 points with street-level detail, starting in south Germany and ending in southern Spain.

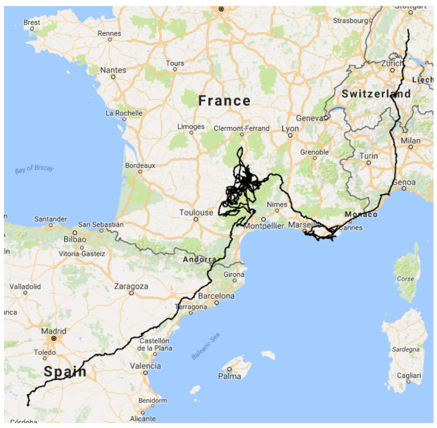

Figure 3.4: Migrating griffon vulture.

Shortcut graphs in the worst case have $\binom{n}{2}$ edges. This means that explicit shortcut graphs in the worst case require quadratic memory. In order to have experiments that are scalable to dense shortcut graphs, we therefore reduce the number of the points in the input curve. We do this by only including the desired number of points at the beginning of the curve.

Furthermore, all experiments presented in this thesis are performed on a 64-bit Intel Core i7-2630QM machine running Windows 10 with 8 gigabytes of DDR3 SDRAM. The source code is written in C# 6.0 and compiled for 64-bit CPU's.

3.3.1 Performance by Curve Length

In this section we evaluate how the length of the input curve impacts the comparative asymptotic performance of using shortcut interval sets instead of explicit shortcut graphs in practice. For this, we choose the error bound for every length of the input curve such that the resulting shortcut graph includes the shortcuts with the 50% smallest errors. The resulting shortcut graph will therefore always have a density of 50%. We choose this density so that there are many shortcuts, yet shortest paths are non-trivial.

We experimentally compare the memory footprint by comparing the number of shortcuts and the number of shortcut intervals. Furthermore, we compare the asymptotic running time in practice of using breadth-first search (BFS) on explicit shortcut graphs, and range queries on shortcut interval sets. The goal of each running-time experiment is to find a shortest path from p_1 to p_n.

The range queries on shortcut intervals are performed using left-leaning red-black trees [22]. The red-black tree [7] is a popular type of self-balancing binary search tree. Although left-leaning red-black trees perform worse compared to regular red-black trees, they are significantly easier to implement and achieve the same asymptotic time-complexity for each operation.

The results of these experiment are presented in Table 3.1.

	Length of the input curve						
	500	1000	2000	3000	4250	5500	7000
Breadth-First Search (sec.)	0.003	0.011	0.049	0.104	0.209	0.379	0.588
Range Queries (sec.)	0.005	0.011	0.027	0.037	0.059	0.078	0.097
Shortcuts ($\times 10^5$)	6.287	25.073	100.151	225.225	451.878	765.613	1225.52
Shortcut Intervals ($\times 10^5$)	0.104	0.163	0.314	0.303	0.699	0.694	0.789

Table 3.1: Running time in seconds of finding a shortest path from p_1 to p_n, and number of shortcuts and shortcut intervals for various lengths of the input curve, on a shortcut graph with a density of 50%.

A first glance at these results reveals that the number of shortcuts grows quadratically in the length of the input curve, whereas the number of shortcut intervals grows linearly, and non-monotonically. We confirm this insight by plotting the number of shortcuts/shortcut intervals against the length of the input curve, as shown in Figure 3.5.

Recall that by using range queries to find shortest paths in shortcut interval sets, we spend time relative to the number of shortcut intervals. Breadth-first search on the other hand spends time for every shortcut it traverses. To investigate how this different allocation of time determines the overall running time of each approach, consider Figure 3.6. We observe that the running time of breadth-first search is quadratic in the length of the input curve, whereas the range queries exhibit near-linear performance.

In conclusion, the results indicate the linear memory footprint of shortcut intervals sets holds true in practice, which in turn yields a significant improvement to the time required to find shortest paths. We foresee this significant compression of the shortcut graph to be an important stepping stone towards constructing min-# simplifications in near-linear time on large data.

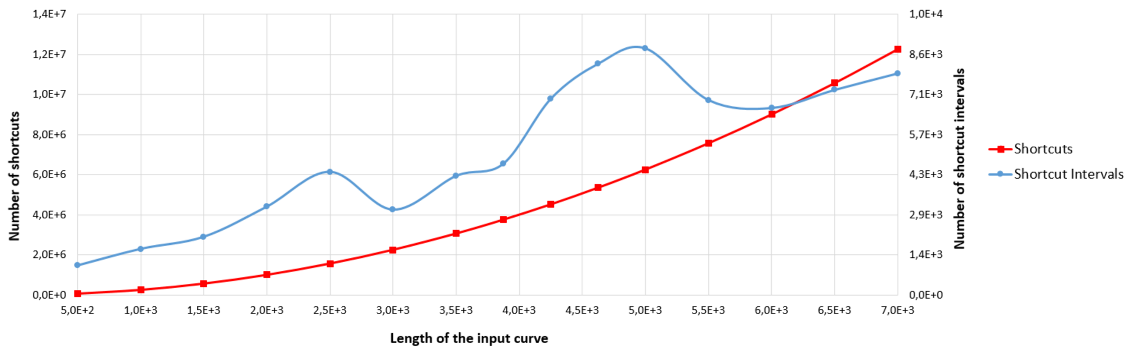

Figure 3.5: Number of shortcuts and shortcut intervals in a shortcut graph with a density of 50% for various lengths of the input curve.

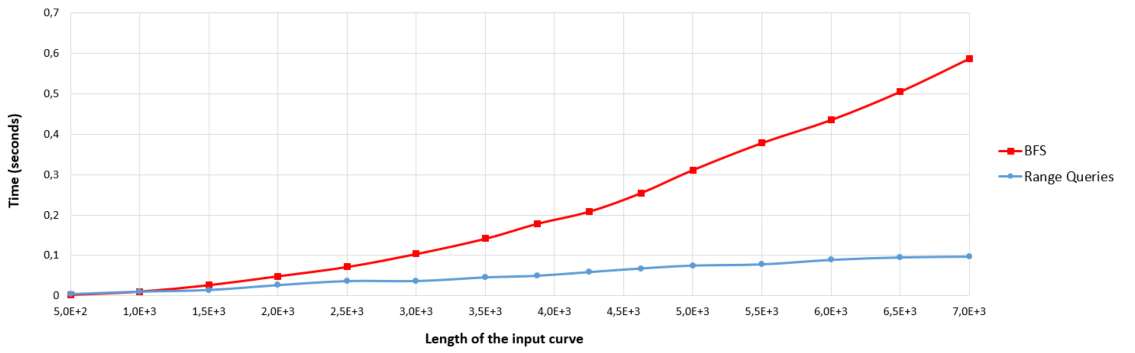

Figure 3.6: Running time of finding a shortest path from p_1 to p_n in a shortcut graph with a density of 50% for various lengths of the input curve.

3.3.2 Performance by Error Bound

The level of compression that can be obtained by using shortcut interval sets depends highly on the density of the shortcut graph. This phenomenon is observable in Figure 3.2. As the error bound grows, the density of the shortcut graph grows, which typically means that the shortcut intervals become coarser. An extreme example of this is a complete shortcut graph, which can be represented with $n-1$ shortcut intervals $[i+1, n]$ for every point $p_i \in \mathcal{C}$ where $1 \leq i < n$.

We perform the same experiments as in Section 3.3.1, except that we vary the error bound instead of the length of the input curve. We fix the length of the input curve to 10.000 points. The results obtained are given in Table 3.2. Note that the last error bound $\varepsilon = 0.095$ yields a complete shortcut graph.

Inspection of these results reveals that the number of shortcut intervals sporadically increases and decreases. As described earlier, this is related to the growth in coarseness among the shortcut intervals as the error bound grows. The relation between the shortcut graph complexity and the error bound is shown in Figure 3.7. We observe monotonic growth in the number of shortcuts, whereas the number of shortcut intervals peeks around $\varepsilon = 0.05$, which corresponds to a shortcut graph density of 80%.

A plot of the running time of both path finding algorithms is given in Figure 3.8. We observe how for small error bounds ($\varepsilon < 0.00015$), breadth-first search on explicit shortcut graphs is faster compared to using range queries on shortcut interval sets. For these error bounds, there are few shortcuts, and path finding via range queries therefore wastes time inserting n points in the annotated balanced binary search tree, without making use of the tree.

To analyze how the shortest path finding performance relates to the number of shortcuts and

	Error bound						
	0.0001	0.001	0.01	0.03	0.06	0.08	0.095
Breadth-First Search (sec.)	0.116	0.465	0.77	1.234	2.367	2.619	2.623
Range Queries (sec.)	0.161	0.183	0.187	0.177	0.17	0.152	0.138
Shortcuts ($\times 10^6$)	2.313	9.682	15.684	24.044	44.991	49.984	49.995
Shortcut Intervals ($\times 10^6$)	0.0197	0.01385	0.01520	0.0151	0.0164	0.0100	0.0100

Table 3.2: Running time in seconds of finding a shortest path from p_1 to p_n, and number of shortcuts and shortcut intervals for 10.000 points and various error bounds.

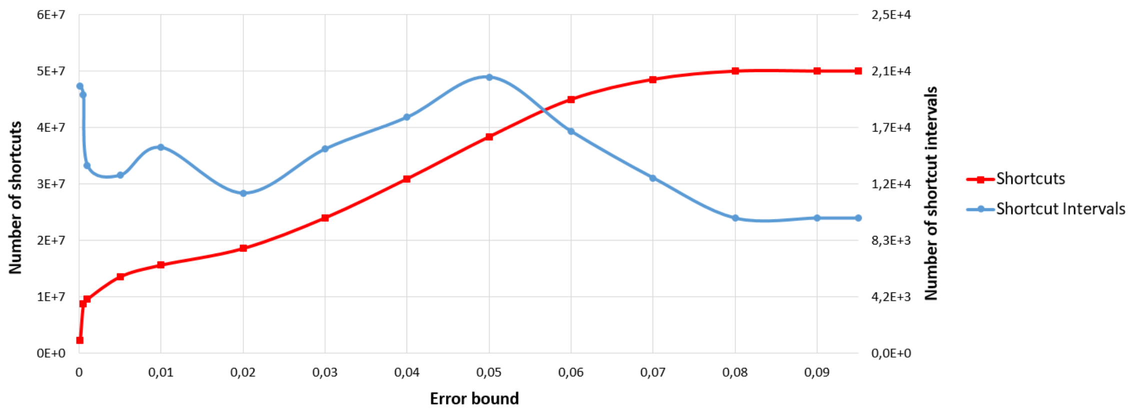

Figure 3.7: Number of shortcuts and shortcut intervals for 10.000 points and various error bounds.

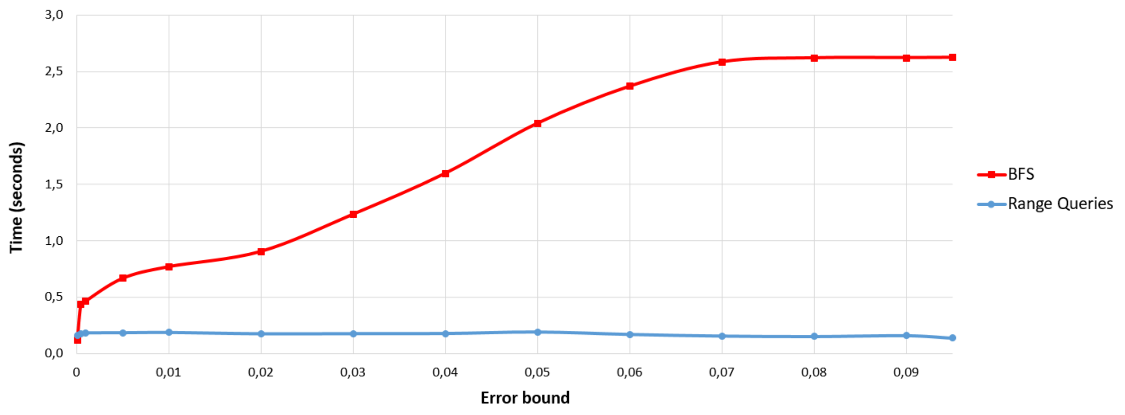

Figure 3.8: Running time of finding a shortest path from p_1 to p_n for 10.000 points and various error bounds.

shortcut intervals, consider Figure 3.9. Here we see the time spent per shortcut and the time spent per shortcut interval, as the error bound grows. In Figure 3.9a, we see that breadth-first search always spends roughly the same amount of time per shortcut. We observe that for range queries on shortcut intervals, the time spent per shortcut decreases as the error bound – and thus the density of the shortcut graph – grows.

In Figure 3.9b we see that finding shortest paths using range queries spends constant time on every shortcut interval, regardless of the error bound. Breadth-first search on the other hand

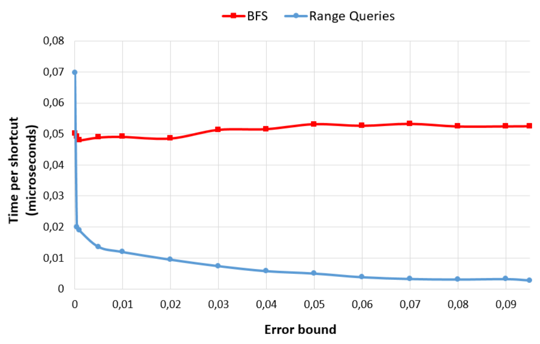

(a) Time per shortcut

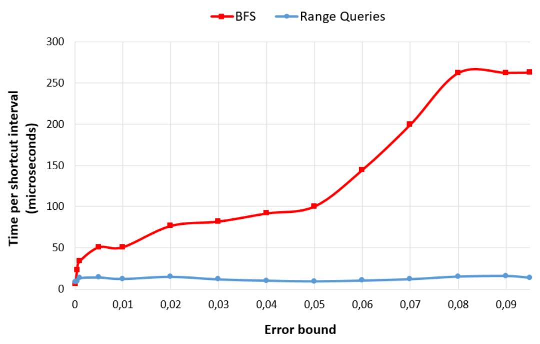

(b) Time per shortcut interval

Figure 3.9: Time spent per shortcut and per shortcut interval in microseconds for finding a shortest path from p_1 to p_n for 10.000 points and various error bounds.

grows to be around 19 times slower per shortcut interval on a complete shortcut graph.

We conclude that shortcut interval sets yield significant benefits both in space- and time complexity for any error bound compared to explicit shortcut graphs. The compression is most effective for larger error bounds that yield dense shortcut graphs. However, for smaller error bounds, the running time of finding shortest paths is highly variable due to the unstable number of shortcut intervals. For highly sparse shortcut graphs, breadth-first search is faster than using range queries on shortcut interval sets, due to the small size of the shortcut intervals.

Chapter 4

Finding Shortcuts for Multiple Scales

Now that we have investigated how to represent the shortcut graph, let us focus on its construction. In this chapter, we will solely consider construction of shortcut graphs under the Hausdorff distance. As mentioned in Chapter 2, the first step of the computational framework by Imai and Iri [16] is to construct a shortcut graph for a polygonal curve $\mathcal{C}$ using a single error bound ε. This problem can be described as follows:

Shortcuts Single Scale
Input: A polygonal curve $\mathcal{C} = \langle p_1, \ldots, p_n \rangle$ in $\mathbb{R}^2$ and an error bound $\varepsilon \geq 0$.
Output: A shortcut graph $G(\mathcal{C}, \varepsilon)$.

However, to facilitate progressive simplification, we wish to construct a sequence of shortcut graphs for a set of error bounds $\mathcal{E} = \langle \varepsilon_1, \ldots, \varepsilon_m \rangle$. We call the corresponding problem Shortcuts Multi-Scale. A naive solution for this problem would be to use any algorithm for solving Shortcuts Single Scale m times to find each shortcut graph independently. However, in the presence of many scales, such an independent construction is likely to cause overhead. We therefore instead determine for each shortcut the maximum error at which it is valid. This problem is defined as follows:

Shortcuts All Scales
Input: A polygonal curve $\mathcal{C} = \langle p_1, \ldots, p_n \rangle$ in $\mathbb{R}^2$.
Output: A set $\mathcal{E}_{max} = \{ \ \mathcal{D}(\langle p_i, \ldots p_j \rangle, \langle p_i, p_j \rangle) \mid 1 \leq i < j \leq n \ \}$.

We call $\mathcal{D}(\langle p_i, \ldots p_j \rangle, \langle p_i, p_j \rangle)$ the *shortcut error* of (p_i, p_j). The solution to this problem can be used to construct a shortcut graph for every error bound $\varepsilon_k \in \mathcal{E}$. We do this by filtering the error values in $\mathcal{E}_{max}$, which takes $O(1)$ time for each potential shortcut. We can thus solve Shortcuts Multi-Scale in $O(n^2 m)$ time from $\mathcal{E}_{max}$.

We first outline a widely used algorithm for solving Shortcuts Single Scale (Section 4.1). Next, we propose a new algorithm for solving Shortcuts All Scales (Section 4.2). Finally, we experimentally evaluate how these algorithms compare in practice (Section 4.3).

4.1 Independent Construction

A well known algorithm for the construction of a single shortcut graph using a fixed error bound under the Hausdorff distance was proposed by Chin and Chan [6]. This algorithm maintains a geometric data structure for every point $p_i \in \mathcal{C}$ that is capable of sequentially determining for any point p_j whether (p_i, p_j) is a shortcut in $O(1)$. One can visualize this data structure as a pie wedge w that has p_i at its center. For every point p_j, (p_i, p_j) is a shortcut if and only if p_j is

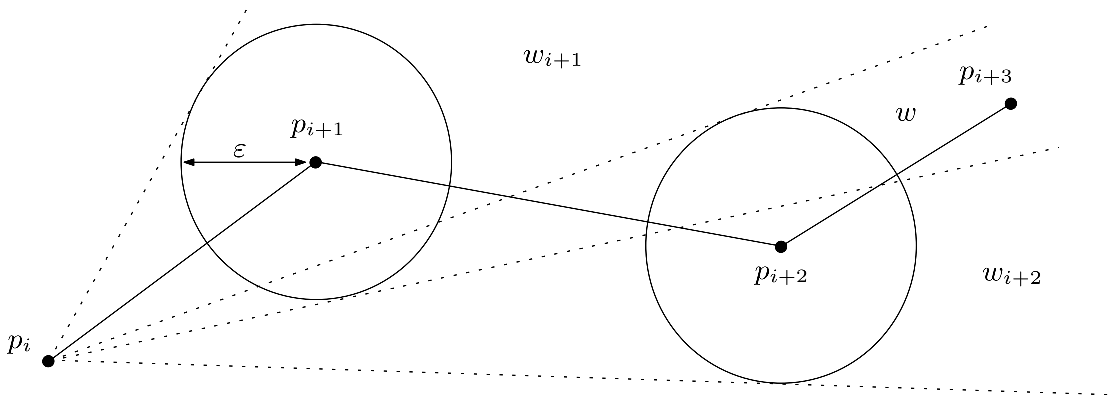

Figure 4.1: Finding shortcuts using wedges.

inside this wedge. After determining this, we intersect the shape of w with the shape of pie wedge w_j. The pie wedge w_j has p_i at its center, and is the smallest wedge that fully includes a circle with radius ε which center is located at p_j. If the resulting intersection of w with w_j is an empty shape, we know that there is no shortcut (p_i, p_k), where $k > j$. An example of this algorithm is shown in Figure 4.1. Here, (p_i, p_{i+1}) and (p_i, p_{i+3}) are shortcuts, and (p_i, p_{i+2}) is not, as it lies outside of w_{i+1}.

However, there is a degenerate case, which is shown in Figure 4.2. Here, we can see that p_{i+4} is inside the wedge w. However, it is clear to see that $dist(p_{i+3}, (p_i, p_{i+4})) \gg \varepsilon$, and thus using Lemma 2.1, we know that (p_i, p_{i+4}) is not actually a shortcut.

Chin and Chan [6] suggested these cases should be handled by first traversing $\mathcal{C}$ from start to end, producing for every point p_i all shortcuts (p_i, p_j) as described above. Next, we do the same but for a reverse traversal of $\mathcal{C}$, producing for every point p_j all shortcuts (p_i, p_j). Finally, these two sets of shortcuts are intersected, which yields the set of edges for shortcut graph $G(\mathcal{C}, \varepsilon)$. For the traversal of $\mathcal{C}$ in the forward direction, we provide pseudo code in Algorithm 4.1.

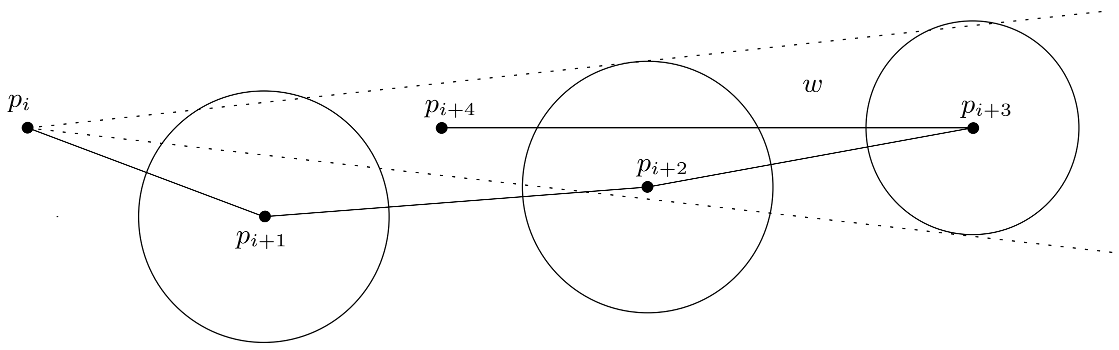

Figure 4.2: A degenerate case where p_{i+4} is in w, yet (p_i, p_{i+4}) is not a shortcut.

Integration of shortcut intervals Recall that in the worst case, there are $\binom{n}{2}$ shortcuts. Therefore, intersecting two sets of shortcuts as described earlier takes $O(n^2)$ time. We can optimize this by using shortcut interval sets, since intersecting any two intervals takes $O(1)$ time, and we have $O(n)$ shortcut intervals in practice. Thus, we can intersect two shortcut interval sets $I'(\mathcal{C}, \varepsilon) = \langle I'_1(\varepsilon), \ldots, I'_n(\varepsilon)\rangle$ and $I''(\mathcal{C}, \varepsilon) = \langle I''_1(\varepsilon), \ldots, I''_n(\varepsilon)\rangle$ in $O(n)$ time by progressively scanning $I'_i(\varepsilon)$ and $I''_i(\varepsilon)$ for intersections in $O(1)$ time for every $p_i \in \mathcal{C}$. An example of such an intersection of $I'_i(\varepsilon)$ and $I''_i(\varepsilon)$ is shown in Figure 4.3. Note that in the worst case we have $O(n^2)$ shortcut intervals, in which case the intersection takes $O(n^2)$ time.

Algorithm 4.1 ChinChan($\mathcal{C}, \varepsilon$)

```
for $i \leftarrow 1$ to $n-1$ do
    $w \leftarrow$ Full plane
    for $j \leftarrow i+1$ to $n$ do
        if $p_j$ inside $w$ then
            Add $(p_i, p_j)$ to $G(\mathcal{C}, \varepsilon)$
        end if
        Intersect $w$ with $w_j$
        if $w$ is empty then
            break
        end if
    end for
end for
return $G(\mathcal{C}, \varepsilon)$
```

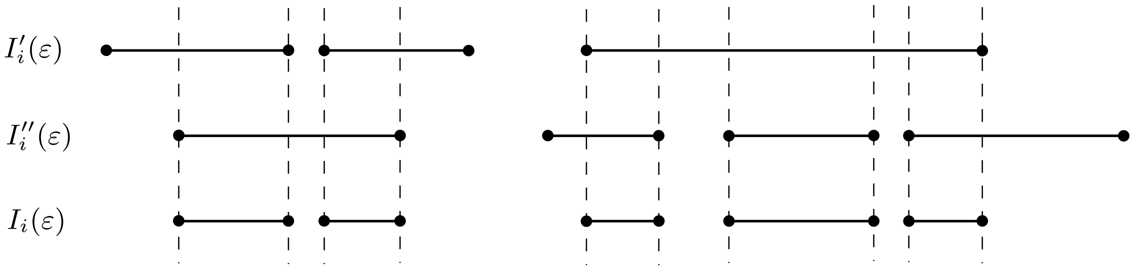

Figure 4.3: Intersecting $I'(\mathcal{C}, \varepsilon)$ and $I''(\mathcal{C}, \varepsilon)$ to obtain $I(\mathcal{C}, \varepsilon)$ for some point p_i.

Running time This algorithm spends $O(1)$ time for every shortcut. Therefore, it solves Shortcuts Single Scale in $O(n^2)$ time, since there is a worst case number of $\binom{n}{2}$ shortcuts.

This algorithm has excellent performance on most real-world data sets when ε is small, because of its ability to prune significant portions of line segments whenever w becomes empty. However, it cannot efficiently be extended to facilitate construction of shortcut graphs for multiple scales, since wedge w can only be used to determine the validity of shortcuts for a single error bound.

4.2 Construction for Arbitrary Scale

Imai and Iri [16] used a brute-force approach of building the shortcut graph under the Hausdorff distance, which can be extended to solve Shortcuts All Scales. The algorithm computes the Hausdorff distance for every line segment (p_i, p_j) where $j > i+1$ by explicitly calculating the maximum distance from any point p_k to (p_i, p_j) for all $i < k < j$. Recall that we can calculate the Hausdorff distance this way, as proven by Lemma 2.1.

This algorithm spends $O(j-i)$ time for any line segment (p_i, p_j) to determine its furthest point distance, where $1 \leq i < j \leq n$. Because there are $\binom{n}{2}$ such line segments, this algorithm solves Shortcuts All Scales with a running time of $O(n^3)$.

In this section we discuss how we can improve the running time of this algorithm by determining the shortcut error of every line segment (p_i, p_j) in $O(\log(j-i))$ time. We do this by maintaining a convex hull $CH \subseteq \mathcal{C}$ for any $p_i \in \mathcal{C}$ in which we incrementally insert all points $p_j \in \mathcal{C}$ where $j > i$.

After inserting some point p_j, we find extreme points X_t^{ij} and X_b^{ij} on the convex hull using the upward normal $\vec{n}_{i,j}$ and downward normal $-\vec{n}_{i,j}$ of line segment (p_i, p_j). An extreme point of a convex hull in the direction of some vector is defined as follows:

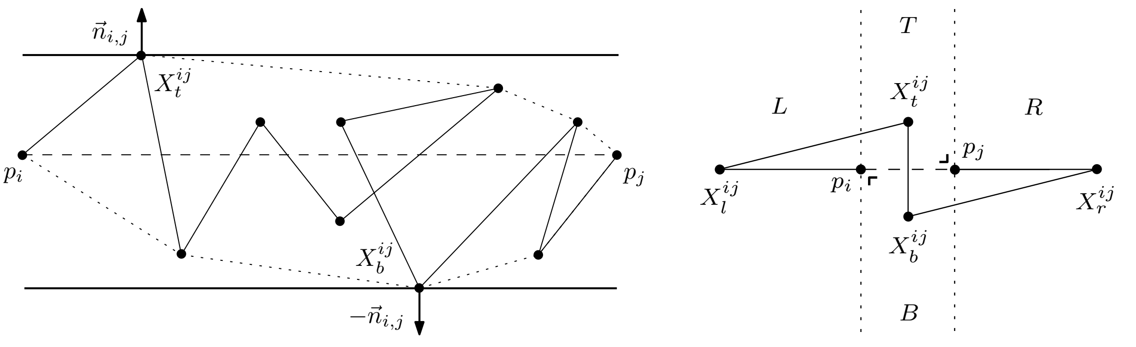

(a) Extreme points of (p_i, p_j) **(b)** Regions of (p_i, p_j)

Figure 4.4: Extreme point queries on the convex hull of $\langle p_i, \ldots, p_j \rangle$.

Extreme Point: *For any convex hull $CH = \langle q_1, \ldots, q_\ell \rangle$, an extreme point of CH in the direction of a vector $\vec{n}$ is any point $x \in CH$ for which there is no point $y \in CH$ such that $\vec{n} \cdot (\vec{y} - \vec{x}) > 0$.*

An example of these extreme points is shown in Figure 4.4a. Here we see a line through X_t^{ij} parallel to (p_i, p_j). The point X_t^{ij} is an extreme point for $\vec{n}_{i,j}$, since all points in CH (and therefore all points in $\mathcal{C}$) are below the line through X_t^{ij} with normal $\vec{n}_{i,j}$.

Although finding both extreme points may seem sufficient to find the furthest point from a given line segment (p_i, p_j), it is not when there are points in the subsequence $\langle p_1, \ldots, p_j \rangle$ that lie to the left of p_i or to the right of p_j within the reference frame of (p_i, p_j). This is illustrated in Figure 4.4b, where we separate the area around the line segment (p_i, p_j) into regions: T(op), B(ottom), L(eft) and R(ight). As shown, the extreme points of (p_i, p_j) are X_t^{ij} and X_b^{ij}, but X_l^{ij} and X_r^{ij} are furthest away from (p_i, p_j). Using extreme point queries, we therefore only find the furthest points in regions T and B. In order to expand the search area to R and L, we need a technique for finding the furthest point X_l^{ij} from p_i in L, and the furthest point X_r^{ij} from p_j in R. This gives us Algorithm 4.2.

Algorithm 4.2 ShortcutsConvexHull($\mathcal{C}$)

```
1:  for $i \leftarrow 1$ to $n-1$ do
2:      $CH \leftarrow$ Empty convex hull
3:      Insert $p_i$ into $CH$
4:      for $j \leftarrow i+1$ to $n$ do
5:          Insert $p_j$ into $CH$
6:          $X_t^{ij} \leftarrow$ Extreme point of $CH$ in the direction $\vec{n}_{i,j}$
7:          $X_b^{ij} \leftarrow$ Extreme point of $CH$ in the direction $-\vec{n}_{i,j}$
8:          $X_l^{ij} \leftarrow$ Furthest point from $p_i$ in $CH$ in region $L$ of $(p_i, p_j)$
9:          $X_r^{ij} \leftarrow$ Furthest point from $p_j$ in $CH$ in region $R$ of $(p_i, p_j)$
10:         $\mathcal{E}_{max}[i][j] \leftarrow \max[dist(X_t^{ij}, (p_i, p_j)), dist(X_b^{ij}, (p_i, p_j)), dist(X_l^{ij}, p_i), dist(X_r^{ij}, p_j)]$
11:     end for
12: end for
13: return $\mathcal{E}_{max}$
```

In order to obtain the desired running time of $O(\log(j-i))$ for any line segment (p_i, p_j), we need to be able to do all queries and insertions in CH in $O(\log(j-i))$ time. To achieve this, we separate the convex hull into a top hull CH_t and a bottom hull CH_b and represent each using a balanced binary search tree without duplicates ordered by the x-coordinates of its points. This allows for finding X_t^{ij} and X_b^{ij} using a binary search on CH_t and CH_b respectively. The insertion of any point p_j into CH is performed by an insertion of p_j in both CH_b and CH_t. Finally, we annotate the nodes of the search trees associated with CH_t and CH_b, and perform a customized range query on these trees to obtain X_l^{ij} and X_r^{ij}. Hence, X_l^{ij} is selected from two furthest point candidates X_{tl}^{ij} and X_{bl}^{ij} from CH_t and CH_b respectively. Similarly, X_r^{ij} is obtained from two candidates X_{tr}^{ij} and X_{br}^{ij}.

We now discuss the details of each operation. We limit our discussion to the top hull $CH_t = \langle q_1, \dots, q_\ell \rangle$, since all operations on CH_b are analogous.

4.2.1 Operations

Inserting p_j Insertion into the top hull CH_t of a point p_j is performed by finding the left-most point $q_l \in CH_t$, and the right-most point $q_r \in CH_t$ such that the line segments (q_l, p_j) and (q_r, p_j) do not pass through CH_t. After we find these two points, we remove all points on the hull in the subsequence $\langle q_{l+1}, \dots, q_{r-1} \rangle$ and insert p_j in between q_l and q_r. Note how this extends the area of the convex hull while maintaining its convexity.

We can find q_l and q_r by doing a binary search on the upward normals of the line segments of CH_t. For example, the binary search for q_r works by finding the right-most point so that the angle of $\vec{n}_{r,j}$ is in between the angles of $\vec{n}_{r-1,r}$ and $\vec{n}_{r,r+1}$. Since the hull is convex, as r increases, $\vec{n}_{r-1,r}$ and $\vec{n}_{r,r+1}$ rotate monotonically clockwise, and $\vec{n}_{r,j}$ rotates monotonically counter-clockwise. At some point the angles of these vectors must converge, and thus a binary search will succeed if q_r exists.

An example of inserting p_j into CH_t is shown in Figure 4.5a. Note how the point between q_l and q_r is removed as a result of the insertion and how the convexity of CH_t is preserved.

If neither q_l nor q_r is found during the binary search, this implies that p_j must lie inside the convex hull, in which case we do not insert p_j. If only q_l was found, we remove all point on the hull after q_l and insert p_j at the end. We do the reverse when only q_r is found.

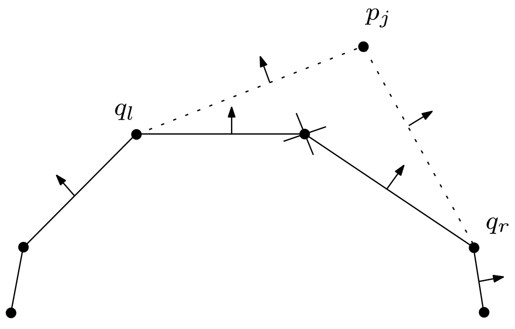

(a) Insertion p_j in between p_l and p_r

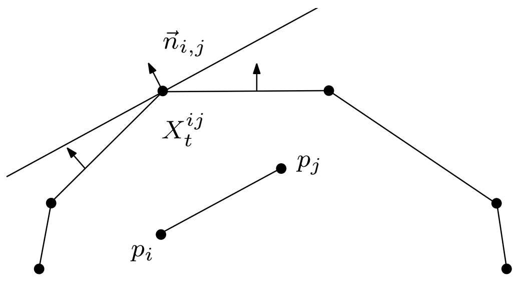

(b) Extreme point in T for (p_i, p_j)

Figure 4.5: Binary search on the convex hull using normals.

Finding X_t^{ij} and X_b^{ij} The extreme point queries in T and B are similar to insertions, and also perform a binary search on the normals of the line segments of the convex hull. Specifically, we find X_t^{ij} in CH_t using upward normal $\vec{n}_{i,j}$ of line segment (p_i, p_j), and we find X_b^{ij} in CH_b using downward normal $-\vec{n}_{i,j}$. This is illustrated for X_t^{ij} in CH_t in Figure 4.5b.

Finding X_l^{ij} In order to efficiently determine X_l^{ij}, we annotate the nodes of the binary search tree of CH_t and CH_b. We annotate any node $q_x \in CH_t$ rooted at subtree T_x with the furthest point from p_i in T_x. An example of such an annotation of the binary search tree of CH_t is shown in Figure 4.6. We now discuss how we can find X_{tl}^{ij} in CH_t.

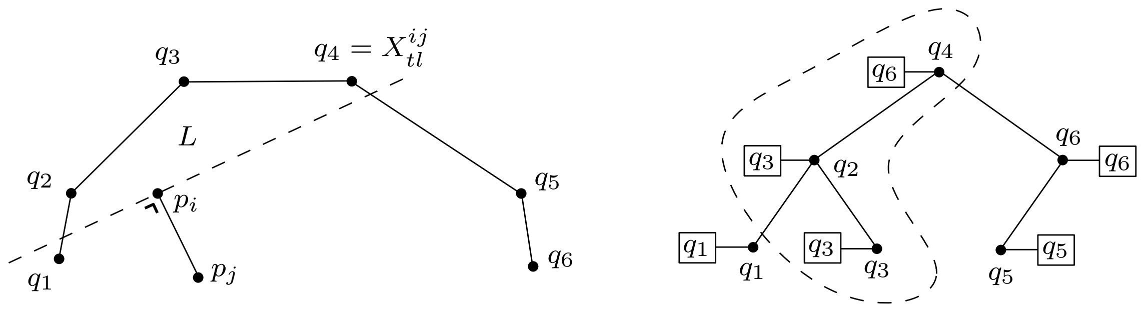

Figure 4.6: CH_t and its annotated binary search tree.

By annotating the search tree of CH_t in this manner, we are able to find X_{tl}^{ij} using a customized range query. We do this by traversing the binary search tree and finding all nodes for which all descendant nodes correspond to points that lie inside L. We then use the annotated point of each such node as a candidate for furthest point from p_i.

We start at the root of the tree, and for every node q_x annotated with point q_a rooted at subtree $T_x = \langle q_l, \ldots, q_r \rangle$, we do the following:

- If both q_l and q_r lie inside L, consider subtree annotation q_a as a furthest point candidate.
- Otherwise:
  - If q_x lies inside L, consider q_x as a furthest point candidate.
  - If either q_l or q_r lies inside L, traverse to both children of q_x.

Note that we only check whether left-most point q_l in T_x, right-most point q_r in T_x, and q_z lie inside L. This is an $O(1)$ operation. The intuition is that in most cases, if the the start and end of a subsequence of points on the hull are inside L, then so are all other points in that subsequence, due to the convexity of the hull. However, this is not always the case when p_i lies horizontally between q_l and q_r. In this scenario, we need to be aware of the following two degenerate cases:

- Figure 4.7a: neither q_l nor q_r lies inside L, and p_j lies below p_i. Only q_x is considered for furthest point from p_i. However, the furthest point from p_i in L may be some other point in T_x and is therefore potentially missed.
- Figure 4.7b: both q_l and q_r lie inside L, and p_j lies above p_i. We obtain the annotation of q_x, which is the furthest point from p_i in T_x. However, not all points in T_x lie inside L.

We handle both cases by consdering the node annotation of q_x and traversing to both children.

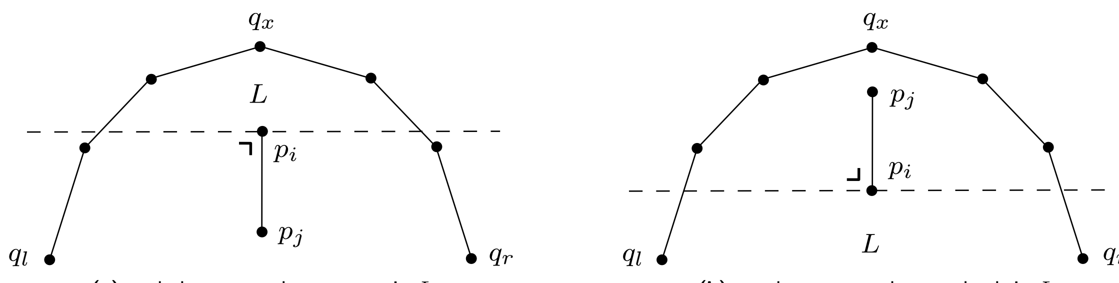

(a) p_j below p_i, and q_l, q_r not in L **(b)** p_j above p_i, and q_l, q_r both in L

Figure 4.7: Degenerate cases where p_i lies horizontally between q_l and q_r.

Finding X_r^{ij} Note that we traverse $\mathcal{C}$ from start to end, and can therefore not directly apply the same approach for finding X_l^{ij} to find X_r^{ij}. We instead apply the same technique used by ChinChan (Algorithm 4.1), which is to run the algorithm a second time using a reversed traversal of $\mathcal{C}$. This means we defer the calculation of the shortcut error until after all furthest point candidates are found.

During the forward traversal of $\mathcal{C}$, we obtain X_t^{ij}, X_b^{ij} and X_l^{ij} at every iteration, whereas during the reverse traversal we only obtain X_r^{ij} at every iteration. After all candidates are found for every line segment, we compute the shortcut error as stated on line 10 of ShortcutsConvexHull.

4.2.2 Running Time

Note how the annotation of the convex hull is much like the annotation of the binary search tree used for finding shortest paths in shortcut interval sets (see Section 3.2). Therefore, the same arguments about running time apply. Because both CH_t and CH_b have at most $O(j-i)$ points when inserting p_j, all binary search tree operations run in $O(\log(j-i))$ time.

Due to the convexity of the hull, all candidates for furthest point from p_i in L or from p_j in R lie on at most one subsequence of points on the convex hull, as shown in Figure 4.8a. The degenerate case shown in Figure 4.7b is the only exception, where there are candidates in two subsequences. However, these subsequences are on both extremes of the tree, as illustrated in Figure 4.8b. For this case we therefore also traverse the children of at most two nodes at each level of the tree. Therefore, the range queries have a time complexity of $O(\log(j-i))$.

We conclude ShortcutsConvexHull solves Shortcuts All Scales with a running time of $O(n^2 \log n)$.

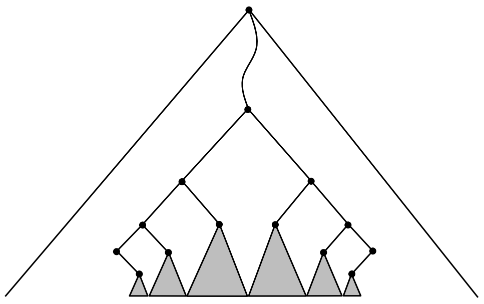
(a) Single subsequence

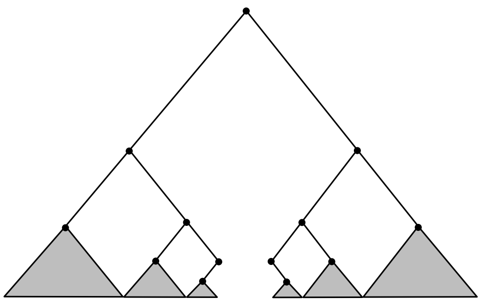
(b) Two subsequences on both extremes

Figure 4.8: Subtrees of CH_t containing closest point candidates for p_i in L.

4.2.3 Correctness

Consider we have a line segment $(p_i, p_j) \in \mathcal{C}$ where $j > i$, and that CH_t and CH_b are the top and bottom parts of the convex hull obtained by incrementally inserting p_i up to p_j. We first prove that the furthest point from (p_i, p_j) in $\langle p_i, \ldots, p_j \rangle$ can be found in CH_t or CH_b.

Lemma 4.1. *If p_k is the furthest point from (p_i, p_j) in the subsequence $\langle p_i, \ldots, p_j \rangle$, then $p_k \in CH_t \cup CH_b$.*

Proof. Assume $p_k \notin CH_t \cup CH_b$. Because CH_t and CH_b are convex and together form a single convex shape, we know that p_k must lie strictly below all line segments of CH_t and strictly above all line segments of CH_b.

Consider the case where the line segment from the closest point from p_k on (p_i, p_j) to p_k goes upwards. We know that by extending this line, it intersects CH_t in some line segment (q_x, q_{x+1}), as sketched in Figure 4.9. Note that either q_x or q_{x+1} must be further away from (p_i, p_j) than p_k, regardless of the geometric configuration. Thus, p_k is not actually the furthest point from (p_i, p_j) in $\langle p_i, \ldots, p_j \rangle$. By contradiction, we obtain that in this case, $p_k \in CH_t \cup CH_b$.

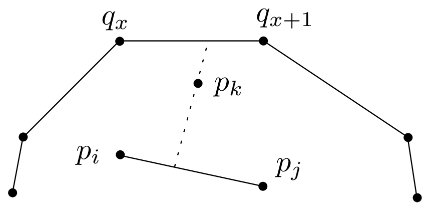

Figure 4.9: Furthest point $p_k \notin CH_t$.

An analogous argument can be given for the case where the perpendicular line from (p_i, p_j) to p_k goes downwards through CH_b. We conclude by contradiction that $p_k \in CH_t \cup CH_b$ always holds. □

Let us prove that among all points on CH_t and CH_b, the set of candidates for the furthest point from (p_i, p_j) found by ShortcutsConvexHull contains the actual furthest point in the hull from (p_i, p_j). We do this by proving that the algorithm identifies the furthest point in each region of (p_i, p_j) (see Figure 4.4b). Let us start with region T.

Lemma 4.2. *X_t^{ij} is the furthest point from (p_i, p_j) in CH_t in region T of (p_i, p_j).*

Proof. Let us define $X_t^{ij} = q_x$. Assume q_x is not the furthest point in CH_t from (p_i, p_j) in region T of (p_i, p_j).

Therefore, there is a point q_y on the hull that lies beyond the line through q_x with normal $\vec{n}_{i,j}$. Due to the convexity of the hull, the line must pass through the hull. Since the normals of the line segments on the hull rotate monotonically, the angle of $\vec{n}_{i,j}$ does not lie in between the angles of $\vec{n}_{x-1,x}$ and $\vec{n}_{x,x+1}$. This implies q_x is not an extreme point, as is illustrated in Figure 4.10a.

By contradiction, we conclude that $q_x = X_t^{ij}$ must be the furthest point in CH_t from (p_i, p_j) in region T of (p_i, p_j). □

An analogous proof can be given to show that X_b^{ij} is the furthest point from (p_i, p_j) in CH_b in region B. We continue with region L.

Lemma 4.3. *X_{tl}^{ij} is the furthest point from p_i in CH_t in region L of (p_i, p_j).*

Proof. Assume the furthest point from p_i in CH_t in region L of (p_i, p_j) is not X_{tl}^{ij}, but rather some other point $q_a \in CH_t$.

We know that q_a is not visited, because otherwise we would have $q_a = X_{tl}^{ij}$ by checking its annotation, yielding a contradiction. Therefore, at some ancestor q_x of q_a, we did not continue on a path down to q_a. We further know that the annotation of q_x is not considered, because otherwise $q_a = X_{tl}^{ij}$, yielding the same contradiction.

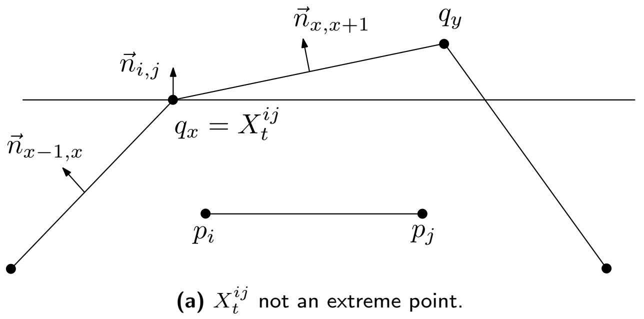

(a) X_t^{ij} not an extreme point.

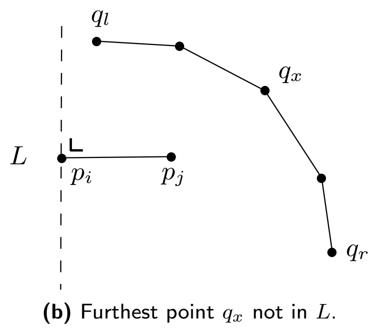

(b) Furthest point q_x not in L.

Figure 4.10: Proving completeness of the furthest point candidates found by Algorithm 4.2.

Thus, both the left-most point q_l and right-most point q_r of the subtree T_x rooted at p_x must lie outside of L, and p_i does not lie in between q_l and q_r. This situation is sketched in Figure 4.10b. Because CH_t is convex, all points in T_x must lie outside of L. This implies q_a lies outside of L, since q_a is a descendant of q_x, and must therefore be in T_x.

By contradiction, we conclude X_{tl}^{ij} must be the furthest point in CH_t from p_i in region L of (p_i, p_j). □

Analogous proofs can be given to prove analogous claims for X_{bl}^{ij}, X_{tr}^{ij} and X_{br}^{ij}.

Theorem 4.4. *Given a polygonal curve $\mathcal{C} = \langle p_1, \ldots, p_n \rangle$, we can compute $\mathcal{H}(\langle p_i, \ldots, p_j \rangle, \langle p_i, p_j \rangle)$ for all $1 \leq i < j \leq n$ in $O(n^2 \log n)$.*

Proof. From Lemma 4.2 and Lemma 4.3, we deduce that the furthest point from (p_i, p_j) in $CH_t \cup CH_b$ must be found by ShortcutsConvexHull. Using Lemma 4.1, it follows that this furthest point from (p_i, p_j) in $CH_t \cup CH_b$ is the furthest point from (p_i, p_j) in $\langle p_i, \ldots, p_j \rangle$. We therefore obtain $\mathcal{E}_{max}[i][j] = \max_{p_k \in \langle p_i, \ldots, p_j \rangle} dist(p_k, (p_i, p_j))$. Correctness follows by Lemma 2.1. □

4.3 Experimental Evaluation

In Section 4.1 we discussed how shortcut interval sets can be exploited to speed up construction of the shortcut graph using ChinChan. In this section, we aim to investigate how this technique performs in practice, with regards to the length of the input curve and the error bound. Furthermore, we explore how well ShortcutsConvexHull performs at constructing shortcut graphs for multiple scales.

For the experimental setup, refer to Section 3.3.

4.3.1 Construction of Shortcut Interval Sets

In this section, we evaluate how the representation of the shortcut graph influences its construction using ChinChan. We start with determining how the length of the input curves influences the running time. We fix the shortcut graph density to 25% by choosing the error bound for every input such that the resulting shortcut graph includes the shortcuts with the 25% smallest errors. The results are listed in Table 4.1.

	Length of the input curve						
	500	1000	1500	2500	3500	4250	5000
Explicit Shortcut Graph (sec.)	0.329	1.267	3.052	8.278	16.125	23.511	32.705
Shortcut Interval Set (sec.)	0.152	0.541	1.247	3.270	5.954	8.703	13.030
Shortcuts ($\times 10^4$)	3.169	12.587	28.256	78.344	154.43	226.15	312.94
Shortcut Intervals ($\times 10^4$)	0.084	0.190	0.242	0.373	0.659	0.868	0.816

Table 4.1: Running time in seconds of ChinChan and the associated number of shortcuts and shortcut intervals for constructing a shortcut graph with 25% density for various lengths of the input curve.

Plotting the running time results against the length of the input curve gives us Figure 4.11. We observe that construction of shortcut interval sets consistently exhibits about 40% of the growth in running time given by the construction of explicit shortcut graphs. Recall that ChinChan constructs explicit shortcut graphs by intersecting two sets of shortcuts. To facilitate this intersection, each of these sets must maintain an index of the shortcuts it contains. No such index needs to be maintained by shortcut interval sets. Thus, insertion of new shortcuts into shortcut interval sets is faster than inserting them into sets that explicitly store shortcuts. The running time improvements are therefore not solely caused by the fast intersection of intervals discussed in Section 4.1

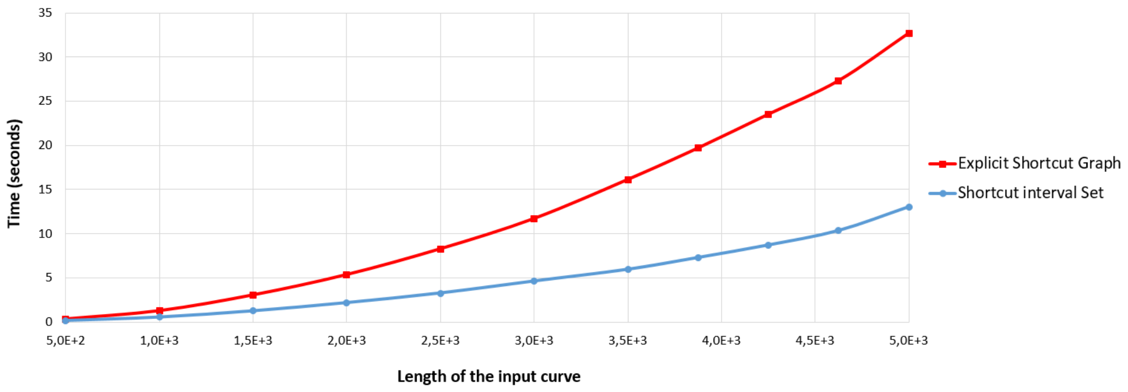

Figure 4.11: Running time in seconds of ChinChan with explicit shortcut graphs versus shortcut interval sets for various lengths of the input curve, and 25% density of the shortcut graph.

Next, we investigate how the density of the shortcut graph influences the construction time. For this, we vary the error bound while fixing the length of the input curve to 3000. The results obtained are given in Table 4.2. Note that the last error bound $\varepsilon = 0.085$ yields a complete shortcut graph.

	Error bound						
	0.001	0.005	0.01	0.03	0.05	0.07	0.085
Explicit Shortcut Graph (sec.)	2.375	11.299	16.881	27.305	37.768	44.705	47.326
Shortcut Interval Set (sec.)	0.945	4.083	5.887	8.929	13.876	15.154	14.101
Shortcuts ($\times 10^4$)	20.698	99.908	161.82	264.17	346.68	430.044	449.85
Shortcut Intervals ($\times 10^4$)	0.499	0.458	0.545	0.458	0.503	0.369	0.300

Table 4.2: Running time in seconds of ChinChan for both shortcut graph representations and the associated number of shortcuts and shortcut intervals for various error bounds and 3000 points.

A plot of these results is given in Figure 4.12. As in Figure 4.11, the construction of shortcut interval sets shows a growth in running time with respect to the error bound that is on average 40% that of the growth exhibited by explicit shortcut graphs.

This relationship on the time complexity is further illustrated by Figure 4.13a, where the time spent per shortcut is plotted against the error bound. We observe that the time spent per shortcut for both representations remains stable as the error bound grows.

Figure 4.13a shows a similar plot of the time spent per shortcut interval. We can see how the time spent per shortcut interval non-monotonically increases as the error bound grows. This is due to the non-monotonic growth of the number of shortcut intervals. As can be seen in Table 4.2, the number of shortcut intervals sporadically increases and decreases as the density of the shortcut graph grows.

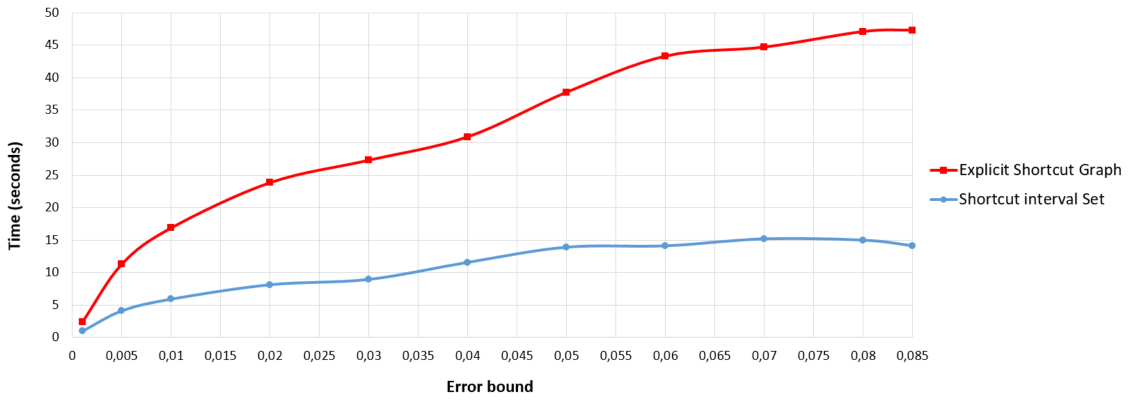

Figure 4.12: Running time in seconds of ChinChan with explicit shortcut graphs versus shortcut interval sets for various error bounds on 3000 points.

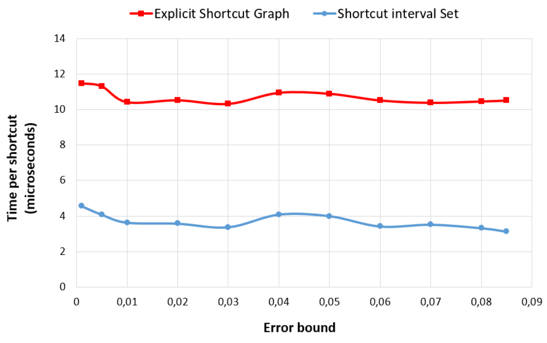

(a) Running time per shortcut

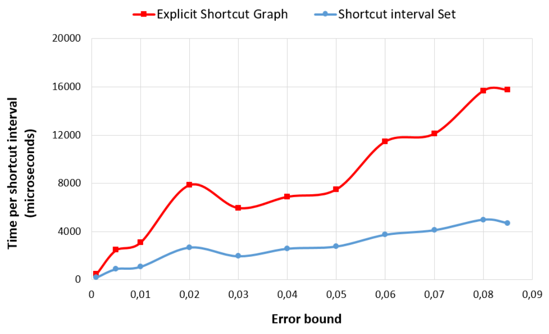

(b) Running time per shortcut interval

Figure 4.13: Time spent per shortcut and per shortcut interval in microseconds by ChinChan with explicit shortcut graphs versus shortcut interval sets for various error bounds and 3000 points.

We conclude that ChinChan is most efficient using shortcut interval sets, yielding significant running time improvements for large input curves. Recall that in Section 3.3, we concluded that shortcut interval sets in practice also yield significant benefits in terms of memory usage, and running time for finding shortest paths. Shortcut interval sets thus yield benefits in each computational aspect of the min-# simplification framework [16].

4.3.2 Construction for Multiple Scales

We described in Section 4.1 how ChinChan has a worst case running time of $O(n^2m)$. Furthermore, in Section 4.2.2 we showed that integrated construction of m shortcut graphs using ShortcutsConvexHull takes $O(n^2 \log n + n^2m)$ time. In this section we investigate how these terms relate to running-time performance in practice, and at what number of scales the initial time investment of $O(n^2 \log n)$ spent by ShortcutsConvexHull to compute all shortcut errors amortizes to be more efficient than ChinChan.

Like the binary search tree used for finding shortest paths in shortcut interval sets (see Section 3.2), we use left-leaning red-black trees [22] to represent the convex hulls CH_t and CH_b of ShortcutsConvexHull. Furthermore, we use the most efficient implementation of ChinChan using shortcut interval sets.

We sample the error bounds from the distribution of shortcut errors of $\mathcal{C}$. We first obtain all shortcut errors using any algorithm to solve Shortcuts All Scales. Next, we sort the errors and linearly sample m error bounds. This yields a shortcut graph $G(\mathcal{C}, \varepsilon_m)$ with a density of 100%. By linearly sampling, the density of the shortcut graphs grows linearly as the scale increases. Recall that ChinChan performs well for small error bounds, and poorly for large error bounds. By sampling up to an error bound that yields a complete shortcut graph, we thus exhaustively capture the strengths and weaknesses of ChinChan.

	Number of scales								
	1	5	10	20	30	40	60	80	100
Convex hulls	285.41	300.27	317.93	335.46	368.20	397.67	455.58	528.11	594.19
Chin-Chan	10.45	45.59	77.59	146.84	216.09	288.04	426.75	579.63	724.74

Table 4.3: Running time in seconds for constructing multiple shortcut interval sets using independent construction by ChinChan versus integrated construction by ShortcutsConvexHull on 3500 points, with error bounds linearly sampled from the smallest to the largest shortcut error.

The running-time measurement are listed in Table 4.3. The corresponding plot is given in Figure 4.14. We observe that the running time of both algorithms is linear in the number of scales. For the construction of a single shortcut graph, ShortcutsConvexHull is 27 times slower than ChinChan. However, ChinChan spends on average 7.2 seconds for every additional error bound, whereas ShortcutsConvexHull spends on average only 3.1 seconds. Therefore, for every additional scale, ShortcutsConvexHull is over twice as efficient as ChinChan. Beyond 65 error bounds, ShortcutsConvexHull is the preferred construction algorithm in terms of running time.

We conclude that ShortcutsConvexHull is only preferable to ChinChan when constructing a large number of shortcut graphs. Its applications are therefore limited to simplification for many levels of detail, such as interactive visualizations with many zoom levels.

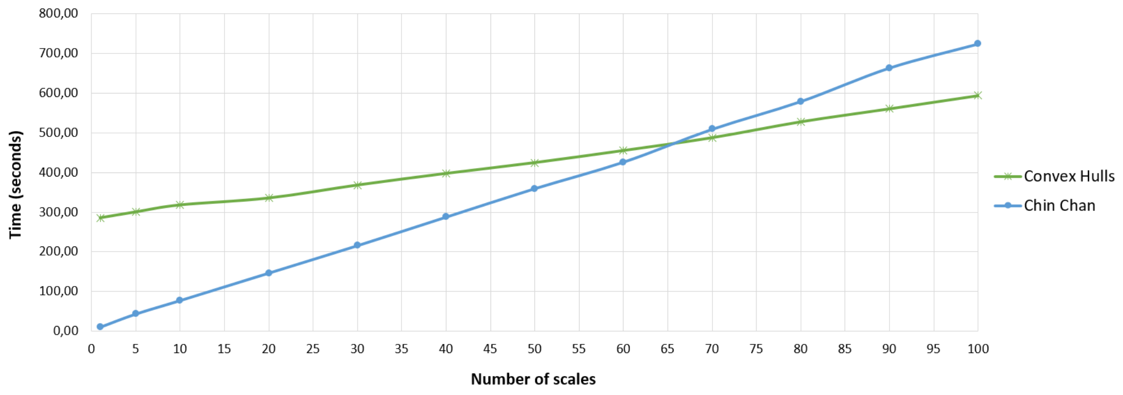

Figure 4.14: Running time in seconds of constructing multiple shortcut interval sets using ChinChan versus ShortcutsConvexHull on 3500 points for various numbers of scales.

Chapter 5

Progressive Simplification of Polygonal Curves

In this chapter we discuss two approaches for solving PROGRESSIVE MIN-#. We propose a progressive simplification algorithm that minimizes the number of points across all scales (Section 5.1). Next, we present two greedy algorithms with better running times that do not provide these guarantees on the simplification size, and show how existing non-progressive algorithms can be extended to greedily compute progressive simplifications (Section 5.2). Finally, we experimentally evaluate how both of these approaches compare, and how they compare to a minimal non-progressive simplification algorithm (Section 5.3).

5.1 An Optimal Algorithm

Recall that a progressive simplification is defined by a set of simplifications for various error bounds on which a monotonic containment relation exists. This means that for any two simplifications $\mathcal{S}_\ell$ and $\mathcal{S}_k$ where $1 \leq \ell \leq k$, $\mathcal{S}_\ell$ must include all points of $\mathcal{S}_k$. Including a shortcut (p_i, p_j) in any simplification $\mathcal{S}_k$ thus has an impact on the structure of all simplifications at a lower scale. Therefore, a global minimum has to be computed on the cumulative size of the simplifications.

We compute this global minimum by associating a cost with including any shortcut in any simplification. Specifically, we have an integer cost $c_{ij}^k \in \mathbb{N}$ associated with including any shortcut (p_i, p_j) from the shortcut graph $G(\mathcal{C}, \varepsilon_k)$ in the simplification $\mathcal{S}_k$. This integer cost represents the minimal combined number of shortcuts $(p_x, p_y) \in \langle p_i, \dots, p_j \rangle$ that will have to be added to any $\mathcal{S}_\ell$ where $1 \leq \ell \leq k$, if we include (p_i, p_j) in $\mathcal{S}_k$. This gives us the following cost function:

$$c_{ij}^k = \begin{cases} 1 & \text{if } (p_i, p_j) \in G(\mathcal{C}, \varepsilon_k) \land k = 1 \\ 1 + \min\limits_{\pi \in \prod_{ij}^{k-1}} \sum\limits_{(p_x, p_y) \in \pi} c_{xy}^{k-1} & \text{if } (p_i, p_j) \in G(\mathcal{C}, \varepsilon_k) \land k > 1 \\ \infty & \text{otherwise} \end{cases}$$

We use $\prod_{ij}^k$ to denote the set of all paths in $G(\mathcal{C}, \varepsilon_k)$ from p_i to p_j.

Using the costs for scale m, we can find $\mathcal{S}_m$ such that the sum of all costs associated with its shortcuts is minimized. Then for any shortcut $(p_i, p_j) \in \mathcal{S}_m$, we can build a simplification for $\langle p_i, \dots, p_j \rangle$ in $\mathcal{S}_{m-1}$ using the costs for scale $m-1$. By chaining all these simplifications together, we obtain $\mathcal{S}_{m-1}$. We continue doing this until we have found $\mathcal{S}_1$.

Determining the cost values as described earlier is possible by adding the costs as weights to

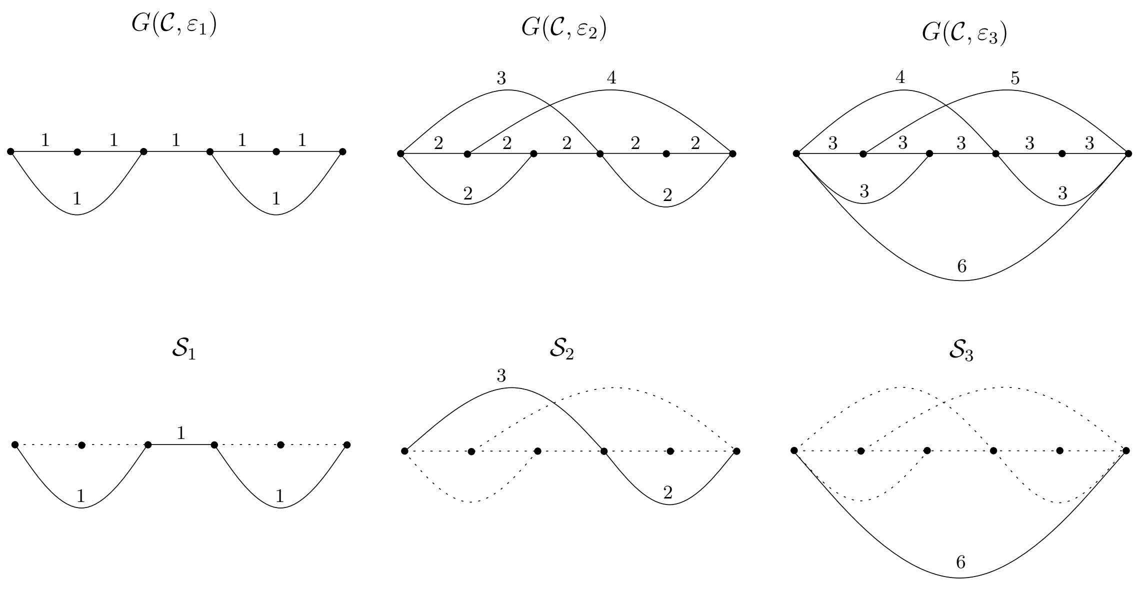
$G(\mathcal{C}, \varepsilon_1)$
$G(\mathcal{C}, \varepsilon_2)$
$G(\mathcal{C}, \varepsilon_3)$
$\mathcal{S}_1$
$\mathcal{S}_2$
$\mathcal{S}_3$

Figure 5.1: Shortcut graphs weighted by cost, and a minimal progressive simplification.

the shortcut graph at every scale. Specifically, any edge (p_i, p_j) in shortcut graph $G(\mathcal{C}, \varepsilon_k)$ has weight c_{ij}^k. The weight of a shortcut c_{ij}^k can then be retrieved by finding a path π in $G(\mathcal{C}, \varepsilon_{k-1})$ from p_i to p_j such that $\sum_{(p_x,p_y)\in\pi} c_{xy}^{k-1}$ is minimized. Similar minimum-weight paths are used to construct the simplifications. In Figure 5.1, a complete example is illustrated which shows how the weights are determined, and how the simplifications are constructed.

From this figure, we observe that for any shortcut (p_i, p_j) at scale k, if $(p_i, p_j) \in G(\mathcal{C}, \varepsilon_{k-1})$, we have $c_{ij}^k = c_{ij}^{k-1} + 1$. Therefore, if a shortcut at scale k is present at scale $k-1$, we can reuse its weight by incrementing it by one. We can prove this as follows:

Lemma 5.1. *For any $1 < k \leq m$ and $n \geq j > i \geq 1$, if $(p_i, p_j) \in G(\mathcal{C}, \varepsilon_{k-1})$, then $c_{ij}^k = c_{ij}^{k-1} + 1$.*

Proof. Assume $(p_i, p_j) \in G(\mathcal{C}, \varepsilon_{k-1})$. Note that $G(\mathcal{C}, \varepsilon_k) \subseteq G(\mathcal{C}, \varepsilon_\ell)$ for all $1 \leq k < \ell \leq m$, because $\varepsilon_\ell \geq \varepsilon_k$. Thus, for all $1 \leq k < \ell \leq m$, any shortcut in $G(\mathcal{C}, \varepsilon_k)$ must also be present in $G(\mathcal{C}, \varepsilon_\ell)$. Because $(p_i, p_j) \in G(\mathcal{C}, \varepsilon_{k-1})$, this implies that $(p_i, p_j) \in G(\mathcal{C}, \varepsilon_k)$.

Case $k = 2$**:** We prove $c_{ij}^2 = c_{ij}^1 + 1$ as follows:

$$\begin{aligned}
c_{ij}^2 &= 1 + \min_{\pi \in \prod_{ij}^1} \sum_{(p_x,p_y)\in\pi} c_{xy}^1 \\
&= 1 + \min_{\pi \in \prod_{ij}^1} \sum_{(p_x,p_y)\in\pi} 1 \\
&= 1 + \min_{\pi \in \prod_{ij}^1} |\pi| \\
&= 1 + 1 && (p_i, p_j) \in \textstyle\prod_{ij}^1 \\
&= c_{ij}^1 + 1
\end{aligned}$$

Case $k > 2$**:** We prove $c_{ij}^k = c_{ij}^{k-1} + 1$ by showing that both the upper and lower bound of c_{ij}^k is equal to $c_{ij}^{k-1} + 1$. Let us start with the upper bound.

$$\begin{aligned} c_{ij}^k &= \min_{\pi \in \prod_{ij}^{k-1}} \sum_{(p_x,p_y)\in\pi} c_{xy}^{k-1} + 1 \\ &\leq \sum_{(p_x,p_y)\in\langle p_i,p_j\rangle} c_{xy}^{k-1} + 1 && (p_i,p_j) \in G(\mathcal{C},\varepsilon_{k-1}) \\ &= c_{ij}^{k-1} + 1 \end{aligned}$$

Now let us prove the lower bound.

$$\begin{aligned} c_{ij}^k &= 1 + \min_{\pi \in \prod_{ij}^{k-1}} \sum_{(p_x,p_y)\in\pi} c_{xy}^{k-1} \\ &= 1 + \min_{\pi \in \prod_{ij}^{k-1}} \sum_{(p_x,p_y)\in\pi} (1 + \min_{\pi' \in \prod_{xy}^{k-2}} \sum_{(p_a,p_b)\in\pi'} c_{ab}^{k-2}) \\ &\geq 1 + 1 + \min_{\pi \in \prod_{ij}^{k-1}} \sum_{(p_x,p_y)\in\pi} \min_{\pi' \in \prod_{xy}^{k-2}} \sum_{(p_a,p_b)\in\pi'} c_{ab}^{k-2} && |\pi| \geq 1 \\ &\geq 1 + 1 + \min_{\pi \in \prod_{ij}^{k-2}} \sum_{(p_x,p_y)\in\pi} c_{xy}^{k-2} \\ &= c_{ij}^{k-1} + 1 \end{aligned}$$

The last inequality holds, since a path from p_i to p_j constructed by concatenating several shortest paths is always at least as long as a single shortest path from p_i to p_j.

We may now conclude that for all $1 < k \leq m$ and $n \geq j > i \geq 1$, we have $c_{ij}^k = c_{ij}^{k-1} + 1$ if $(p_i, p_j) \in G(\mathcal{C}, \varepsilon_{k-1})$. □

We can use this result to efficiently assign a weight to any shortcut that was encountered at an earlier scale, without recomputing a shortest path. The pseudo-code of the resulting algorithm is given in Algorithm 5.1.

Weighted Simplifications Recall that for Weighted Progressive Min-#, we are given positive weights $\mathcal{W} = \langle w_1, \ldots, w_m \rangle$ in $\mathbb{R}$ and need to minimize $\sum_{k=1}^m w_k |\mathcal{S}_k|$. We can trivially extend the cost function c_{ij}^k to facilitate solving this problem. Specifically, we assign a cost of w_k (instead of 1) to every line segment in any simplification $\mathcal{S}_k$, as follows:

$$c_{ij}^k = \begin{cases} w_k & \text{if } (p_i,p_j) \in G(\mathcal{C},\varepsilon_k) \wedge k = 1 \\ w_k + \min_{\pi \in \prod_{ij}^{k-1}} \sum_{(p_x,p_y)\in\pi} c_{xy}^{k-1} & \text{if } (p_i,p_j) \in G(\mathcal{C},\varepsilon_k) \wedge k > 1 \\ \infty & \text{otherwise} \end{cases}$$

5.1.1 Optimization

In this section we explore (potential) techniques for optimizing the running time of ImaiIriProgressive.

Determining shortcut cost A naive technique for finding a shortest path on line 9 is to run any single-source shortest path algorithm for every shortcut (p_i, p_j). Because a shortcut graph contains at most $\binom{n}{2}$ shortcuts, any such algorithm would run in at least $O(n^2)$ time. However, this approach potentially discards shortest path information that can be reused.

Algorithm 5.1 ImaiIriProgressive($\mathcal{C}$, $\mathcal{E}$)

```
1: $G(\mathcal{C},\varepsilon_1),\dots,G(\mathcal{C},\varepsilon_m) \leftarrow$ Shortcuts Multi-Scale($\mathcal{C},\mathcal{E}$)
2: for $k \leftarrow 1$ to $m$ do
3:     for each $(p_i,p_j)$ in $G(\mathcal{C},\varepsilon_k)$ do
4:         if $k = 1$ then
5:             $c_{ij}^k \leftarrow 1$
6:         else if $(p_i,p_j) \in G(\mathcal{C},\varepsilon_{k-1})$ then
7:             $c_{ij}^k \leftarrow 1 + c_{ij}^{k-1}$
8:         else
9:             $c_{ij}^k \leftarrow 1$ + weight of the shortest path from $p_i$ to $p_j$ in $G(\mathcal{C},\varepsilon_{k-1})$
10:        end if
11:    end for
12: end for
13: for $k \leftarrow m$ to 1 do
14:    if $k = m$ then
15:        $\mathcal{S}_k \leftarrow$ shortest path from $p_1$ to $p_n$ in $G(\mathcal{C},\varepsilon_k)$
16:    else
17:        for each $(p_i,p_j)$ in $\mathcal{S}_{k+1}$ do
18:            $\mathcal{S}_k \leftarrow \mathcal{S}_k \cup$ shortest path from $p_i$ to $p_j$ in $G(\mathcal{C},\varepsilon_k)$
19:        end for
20:    end if
21: end for
22: return $\langle \mathcal{S}_1,\dots,\mathcal{S}_m \rangle$
```

Dijkstra's algorithm [9] takes any source node u in a graph $G = (V,E)$ and builds a data structure in $O(|V|\log|V| + |E|)$ time which holds the shortest path distance from u to any target node v. This data structure can be used to construct any of these shortest paths in $O(|V|)$ time. If we run Dijkstra's algorithm every time we reach line 9, we obtain an amortized running time of $O(n^4)$. This is the case since we need to find a weight for a worst case total of $O(n^2)$ shortcuts.

Now consider we instead build this data structure for every scale k only once for every p_i for which there exists some shortcut $(p_i,p_j) \in G(\mathcal{C},\varepsilon_k)$ where $(p_i,p_j) \notin G(\mathcal{C},\varepsilon_{k-1})$. This yields $O(n)$ data structures from which the shortest path for any shortcut at scale k can be obtained in $O(n)$ time. Constructing each data structure takes $O(n^2)$ time, and thus we have a total worse-case running time of $O(n^3m)$.

Integration of shortcut intervals Note that the algorithm to find shortest paths in shortcut interval sets presented in Section 3.2 is not limited to unweighted shortcuts, and can trivially be extended to find paths with lowest weight. We assign a weight w to every shortcut interval $[x,y] \in I_i(\varepsilon)$ for some point p_i, such that every shortcut (p_i,p_j) has weight w where $x \le j \le y$.

By weighting the intervals, we potentially fragment an unweighted interval into many weighted intervals. Therefore, to effectively employ weighted shortcut interval sets, we need most consecutive shortcuts (p_i,p_j) and (p_i,p_{j+1}) to share the same weight.

In Figure 5.2 we see a heat map of the costs of shortcuts in $G(\mathcal{C},\varepsilon_m)$ given by ImaiIriProgressive in practice. The rows and columns correspond to the points in $\mathcal{C}$. Each cell i,j is colored according to the cost c_{ij}^m of

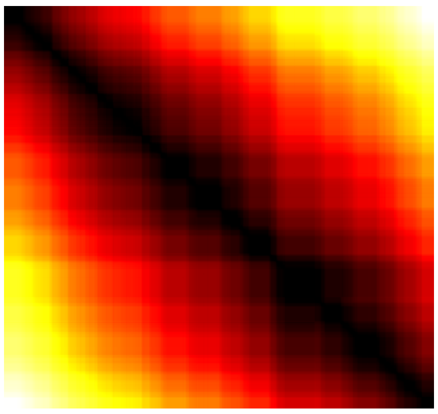
Figure 5.2: Heat map of the shortcut costs in $G(\mathcal{C},\varepsilon_m)$. From low to high cost: black, red, yellow, white.

shortcut (p_i, p_j). Although we observe many regions with a similar color, analysis shows that almost all consecutive shortcuts have a slightly different cost. Therefore, by using weighted shortcut interval sets in ImaiIriProgressive using the costs of the shortcuts, we have $O(n^2)$ weighted intervals in practice. This means no running time advantages can be obtained by using shortcut interval sets for this algorithm.

5.1.2 Correctness

As in the correctness proof of Single Scale min-# given in Section 2.3, we prove the correctness of ImaiIriProgressive by arguing that its output is both valid and minimal. Specifically, the combined number of points should be minimized while having a sequence of simplifications among which there exists a monotonic containment relation. Furthermore, each simplification $\mathcal{S}_k$ should not violate the maximum error ε_k.

Consider $\langle \mathcal{S}_1, \ldots, \mathcal{S}_m \rangle$ is the progressive simplification produced by ImaiIriProgressive for some polygonal curve $\mathcal{C}$ and set of error bounds $\mathcal{E}$. Enforcement of the monotonic containment relation follows directly from the structure of the algorithm. Lines 17-19 impose that for any $1 \leq k < m$ and shortcut $(p_i, p_j) \in \mathcal{S}_{k+1}$, there exists a subsequence $\langle p_i, \ldots, p_j \rangle \sqsubseteq \mathcal{S}_k$. We therefore must have $\mathcal{S}_{k+1} \sqsubseteq \mathcal{S}_k$.

Furthermore, by applying Lemma 2.3, we deduce that each simplification $\mathcal{S}_k$ does not violate the error bound ε_k.

It remains to be shown that the cumulative size of all simplifications is minimal. To this end, we define the following for any $n \geq j > i \geq 1$ and $1 \leq k \leq m$:

$$\mathcal{S}_k^{ij} = \{\ (p_x, p_y) \in \mathcal{S}_k \mid x \leq i < j \leq y\ \}$$

Intuitively, this definition includes all line segments of $\mathcal{S}_k$ that span the subcurve $\langle p_i, \ldots, p_j \rangle$. Let us now prove that the cost of a shortcut (p_i, p_j) in $G(\mathcal{C}, \varepsilon_k)$ is the same as the combined number of links for subsequence $\langle p_i, \ldots, p_j \rangle$ in all simplifications from scale 1 to k.

Lemma 5.2. *For any $1 \leq k \leq m$ and $n \geq j > i \geq 1$, if $(p_i, p_j) \in \mathcal{S}_k$, then $c_{ij}^k = \sum_{\ell=1}^{k} |\mathcal{S}_\ell^{ij}|$.*

Proof. We show $c_{ij}^k = \sum_{\ell=1}^{k} |\mathcal{S}_\ell^{ij}|$ by induction on k using the following induction hypothesis:

$$\text{For any } n \geq y > x \geq 1, \text{ if } (p_x, p_y) \in \mathcal{S}_k, \text{ then } c_{xy}^k = \sum_{\ell=1}^{k} |\mathcal{S}_\ell^{xy}| \tag{IH}$$

Base $k = 1$: Take any shortcut $(p_i, p_j) \in \mathcal{S}_1$. This implies $(p_i, p_j) \in G(\mathcal{C}, \varepsilon_1)$. Furthermore, we know $\mathcal{S}_1^{ij} = \{(p_i, p_j)\}$, so $|\mathcal{S}_1^{ij}| = 1$. We derive the following:

$$c_{ij}^1 = 1 = \sum_{\ell=1}^{k} 1 = \sum_{\ell=1}^{k} |\mathcal{S}_1^{ij}|$$

Step $k > 1$: Take any line segment $(p_i, p_j) \in \mathcal{S}_{k+1}$. This implies $(p_i, p_j) \in G(\mathcal{C}, \varepsilon_{k+1})$, and $\mathcal{S}_{k+1}^{ij} = \{(p_i, p_j)\}$, so $|\mathcal{S}_{k+1}^{ij}| = 1$.

Consider any $1 \leq \ell \leq k$ and a path $\pi \in \prod_{ij}^k$ such that $\sum_{(p_x,p_y)\in\pi} |\mathcal{S}_\ell^{xy}|$ is minimal. We derive that $\pi = \mathcal{S}_\ell^{ij}$, such that $\mathcal{S}_\ell^{xy}$ is minimal for all $(p_x, p_y) \in \pi$. Note that $\pi = \mathcal{S}_\ell^{ij} \subseteq G(\mathcal{C}, \varepsilon_\ell) \subseteq G(\mathcal{C}, \varepsilon_k)$, since $\varepsilon_k \geq \varepsilon_\ell$. From this we may conclude that π is both in $\prod_{ij}^\ell$ and $\prod_{ij}^k$. From this it follows that:

$$\min_{\pi\in\prod_{ij}^k} \sum_{(p_x,p_y)\in\pi} |\mathcal{S}_\ell^{xy}| = \min_{\pi\in\prod_{ij}^\ell} \sum_{(p_x,p_y)\in\pi} |\mathcal{S}_\ell^{xy}| \tag{5.1}$$

Furthermore, from $\pi = \mathcal{S}_\ell^{ij}$ we can derive that $\mathcal{S}_\ell^{xy} \cap \mathcal{S}_\ell^{yz} = \emptyset$ for any (p_x, p_y) and (p_y, p_z) in π. Thus, combining $\mathcal{S}_\ell^{xy}$ for all $(p_x, p_y) \in \pi$ yields a non-overlapping sequence of shortcuts from p_i to p_j. This gives us:

$$\min_{\pi \in \prod_{ij}^{\ell}} \sum_{(p_x,p_y)\in\pi} |\mathcal{S}_\ell^{xy}| = |\mathcal{S}_\ell^{ij}| \tag{5.2}$$

We may now derive the following:

$$\begin{aligned}
c_{ij}^{k+1} &= 1 + \min_{\pi \in \prod_{ij}^{k}} \sum_{(p_x,p_y)\in\pi} c_{xy}^{k} \\
&= 1 + \min_{\pi \in \prod_{ij}^{k}} \sum_{(p_x,p_y)\in\pi} \sum_{\ell=1}^{k} |\mathcal{S}_\ell^{xy}| && \text{IH} \\
&= 1 + \sum_{\ell=1}^{k} \min_{\pi \in \prod_{ij}^{\ell}} \sum_{(p_x,p_y)\in\pi} |\mathcal{S}_\ell^{xy}| && \text{Equation 5.1} \\
&= 1 + \sum_{\ell=1}^{k} |\mathcal{S}_\ell^{ij}| && \text{Equation 5.2} \\
&= \sum_{\ell=1}^{k+1} |\mathcal{S}_\ell^{ij}| && |\mathcal{S}_{k+1}^{ij}| = 1
\end{aligned}$$

Note that we can apply the induction hypothesis, because $(p_x, p_y) \in \mathcal{S}_k$ as stated on line 18 of ImaiIriProgressive. We conclude $c_{ij}^k = \sum_{\ell=1}^{k} |\mathcal{S}_\ell^{ij}|$ if $(p_i, p_j) \in \mathcal{S}_k$ for all $1 \le k \le m$. □

Theorem 5.3. *Given a polygonal curve $\mathcal{C}$ and set of error bounds $\mathcal{E}$, a minimal progressive simplification can be computed in $O(n^3 m)$ time under distance measures for which the validity of a shortcut can be determined in $O(n)$ time, such as Fréchet, Hausdorff and area-based measures.*

Proof. It remains to be proven that the cumulative size of the simplifications computed by ImaiIri-Progressive is minimal. Let $\langle \mathcal{S}_1', \ldots, \mathcal{S}_m' \rangle$ be a minimal progressive simplification, and let $\langle \mathcal{S}_1, \ldots, \mathcal{S}_m \rangle$ be the simplification computed by ImaiIriProgressive. We derive the following:

$$\begin{aligned}
\min_{\pi \in \prod_{1n}^{m}} \sum_{(p_x,p_y)\in\pi} c_{xy}^{m} &= \min_{\pi \in \prod_{1n}^{m}} \sum_{(p_x,p_y)\in\pi} \sum_{\ell=1}^{m} |\mathcal{S}_\ell^{xy}| && \text{Lemma 5.2} \\
&= \sum_{\ell=1}^{m} \min_{\pi \in \prod_{1n}^{\ell}} \sum_{(p_x,p_y)\in\pi} |\mathcal{S}_\ell^{xy}| && \text{Equation 5.1} \\
&= \sum_{\ell=1}^{m} |\mathcal{S}_\ell^{1n}| && \text{Equation 5.2} \\
&= \sum_{\ell=1}^{m} |\mathcal{S}_\ell|
\end{aligned}$$

Note that we can apply Lemma 5.2, since $(p_x, p_y) \in \mathcal{S}_m$, as stated on line 15 of ImaiIriProgress-ive. We observe that the cumulative size of the solution produced by the algorithm constitutes a minimization of the cost function. Therefore, the output of ImaiIriProgressive is a combination of paths in the shortcut graphs $G(\mathcal{C}, \varepsilon_1), \ldots, G(\mathcal{C}, \varepsilon_m)$ among which there exists a monotonic containment relation, such that the combined length is minimal.

Furthermore, by following the same reasoning as in the proof of Lemma 2.4, we know that every $\mathcal{S}'_\ell \in \langle \mathcal{S}'_1, \dots, \mathcal{S}'_m \rangle$ has to be a path in $G(\mathcal{C}, \varepsilon_\ell)$.

From these two claims we conclude $\sum_{\ell=1}^{m} |\mathcal{S}_\ell| \leq \sum_{\ell=1}^{m} |\mathcal{S}'_\ell|$. □

Note that these proofs also apply if we extend the cost function to solve the weighted progressive simplification problem WEIGHTED PROGRESSIVE MIN-#, as described in Section 5.1. Therefore, by Theorem 5.3 and Lemma 2.2, we can deduce the following:

Corollary 5.4. *Given a polygonal curve $\mathcal{C}$, a continuous progressive simplification can be computed in $O(n^5)$ time under distance measures for which the validity of a shortcut can be determined in $O(n)$ time, such as Fréchet, Hausdorff and area-based measures.*

5.2 Greedy Construction Techniques

Because the global minimization of the cumulative simplification size of PROGRESSIVE MIN-# is complex, we investigate two techniques for solving this problem where no requirements are placed on the size of the simplifications. Instead of searching for a global minimum of the combined simplification size, we greedily build the simplifications scale by scale, finding local minima while maintaining the monotonic containment. The simplest way is by building the simplifications from the bottom up, or from the top down. In this section we explore these techniques and discuss how they can be integrated with existing single-scale simplification algorithms.

5.2.1 Top-down Construction

By constructing simplifications from the top down, we employ the divide-and-conquer design paradigm. At every scale k, we divide $\mathcal{C}$ into subcurves by simplification with error bound ε_k. Next, on scale $k-1$, we simplify each of these subcurves using ε_{k-1}, thereby generating more fine-grained subcurves of $\mathcal{C}$. Note that we have already seen this technique in IMAIIRIPROGRESSIVE. The difference is that we greedily choose a simplification $\mathcal{S}_m$ by finding a shortest path in the *unweighted* shortcut graph $G(\mathcal{C}, \varepsilon_m)$. The simplification $\mathcal{S}_{m-1}$ is then found by concatenating all greedily chosen shortest paths from p_i to p_j for every $(p_i, p_j) \in \mathcal{S}_m$. We continue this process until we have found $\mathcal{S}_1$. This gives us Algorithm 5.2.

Algorithm 5.2 IMAIIRITOPDOWN($\mathcal{C}$, $\mathcal{E}$)

```
 1: $G(\mathcal{C},\varepsilon_1),\dots,G(\mathcal{C},\varepsilon_m) \leftarrow$ SHORTCUTS MULTI-SCALE$(\mathcal{C},\mathcal{E})$
 2: for $k \leftarrow m$ to $1$ do
 3:     if $k = m$ then
 4:         $\mathcal{S}_k \leftarrow$ shortest path from $p_1$ to $p_n$ in $G(\mathcal{C},\varepsilon_k)$
 5:     else
 6:         for each $(p_i,p_j)$ in $\mathcal{S}_{k+1}$ do
 7:             $\mathcal{S}_k \leftarrow \mathcal{S}_k \cup$ shortest path from $p_i$ to $p_j$ in $G(\mathcal{C},\varepsilon_k)$
 8:         end for
 9:     end if
10: end for
11: return $\langle \mathcal{S}_1,\dots,\mathcal{S}_m \rangle$
```

Running time The running time is bound by the time spent solving SHORTCUTS MULTI-SCALE($\mathcal{C}, \mathcal{E}$), giving us $O(n^2 m)$ time (see Section 4.1) or $(n^2 \log n + n^2 m)$ time (see Section 4.2).

Optimization Due to the greedy selection of any simplification and the monotonic containment relation among the simplifications, potentially many shortcuts are never considered. For any scale $1 \leq k < m$ and shortcut $(p_x, p_y) \in \mathcal{S}_{k+1}$, we find a simplification of $\langle p_x, \ldots, p_y \rangle$ in $G(\mathcal{C}, \varepsilon_k)$. This means that any shortcut $(p_i, p_j) \in G(\mathcal{C}, \varepsilon_k)$ can never be included in $\mathcal{S}_k$ if $j > x > i$ or $j > y > i$.

We can therefore optimize the algorithm by not considering these shortcuts when constructing the shortcut graphs. Instead of solving Shortcuts Multi-Scale, we solve Shortcuts Single Scale at every scale k using an algorithm that prunes the search space whenever possible.

We extend the shortcut graph construction algorithm by Chin and Chan [6] (Section 4.1). Recall that we construct $G(\mathcal{C}, \varepsilon_k)$ by intersecting two sets of shortcuts obtained by traversing $\mathcal{C}$ in both directions. When traversing $\mathcal{C}$ from start to end, we skip from p_i to p_{i+1} whenever we reach a shortcut (p_i, p_j) such that $i < y < j$ for a line segment $(p_x, p_y) \in \mathcal{S}_{k+1}$. Conversely, when traversing from the end to the start of $\mathcal{C}$, we skip from p_j to p_{j-1} whenever we consider a shortcut (p_i, p_j) such that $i < x < j$ for a line segment $(p_x, p_y) \in \mathcal{S}_{k+1}$. These two types of pruning are illustrated in Figure 5.3.

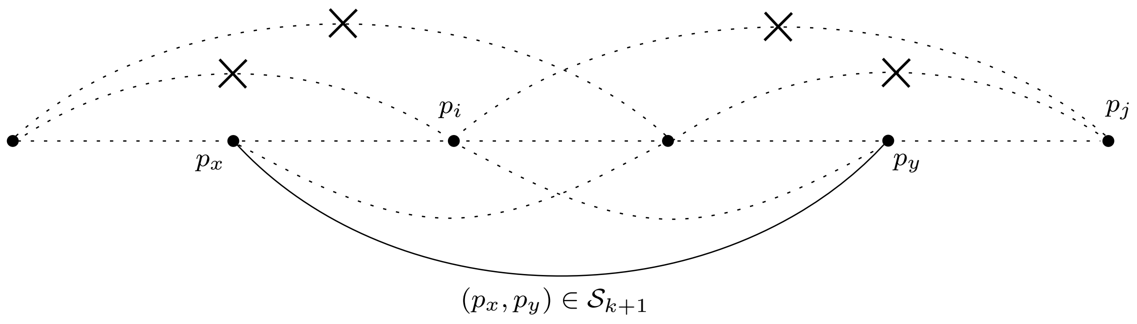

Figure 5.3: Pruning the search space for shortcut graph $G(\mathcal{C}, \varepsilon_k)$.

5.2.2 Bottom-up Construction

By taking greedy choices from the bottom up, we start at the lowest scale with the smallest error bound, thereby starting with the least aggressive greedy choice. Construction at any scale k works by finding a shortest paths from p_1 to p_n in $G(\mathcal{C}, \varepsilon_k)$, and removing all nodes and edges in $G(\mathcal{C}, \varepsilon_{k+1})$ associated with any point $p_i \notin \mathcal{S}_k$, thereby directly imposing $\mathcal{S}_{k+1} \sqsubseteq \mathcal{S}_k$. This is illustrated in Figure 5.4. The algorithm's pseudo code is presented in Algorithm 5.3.

Algorithm 5.3 ImaiIriBottomUp($\mathcal{C}$, $\mathcal{E}$)

```
1: $G(\mathcal{C}, \varepsilon_1), \ldots, G(\mathcal{C}, \varepsilon_m) \leftarrow$ Shortcuts Multi-Scale($\mathcal{C}, \mathcal{E}$)
2: for $k \leftarrow 1$ to $m$ do
3:     $\mathcal{S}_k \leftarrow$ shortest path from $p_1$ to $p_n$ in $G(\mathcal{C}, \varepsilon_k)$
4:     for each $p_k$ in $\mathcal{C}$ do
5:         if $p_i \notin \mathcal{S}_k$ then
6:             Remove $p_i$ from $G(\mathcal{C}, \varepsilon_{k+1})$
7:         end if
8:     end for
9: end for
10: return $\langle \mathcal{S}_1, \ldots, \mathcal{S}_m \rangle$
```

Running time As for ImaiIriTopDown, the running time is bound by the time spent constructing the shortcut graphs, yielding $O(n^2 m)$ (Section 4.1) or $(n^2 \log n + n^2 m)$ (Section 4.2).

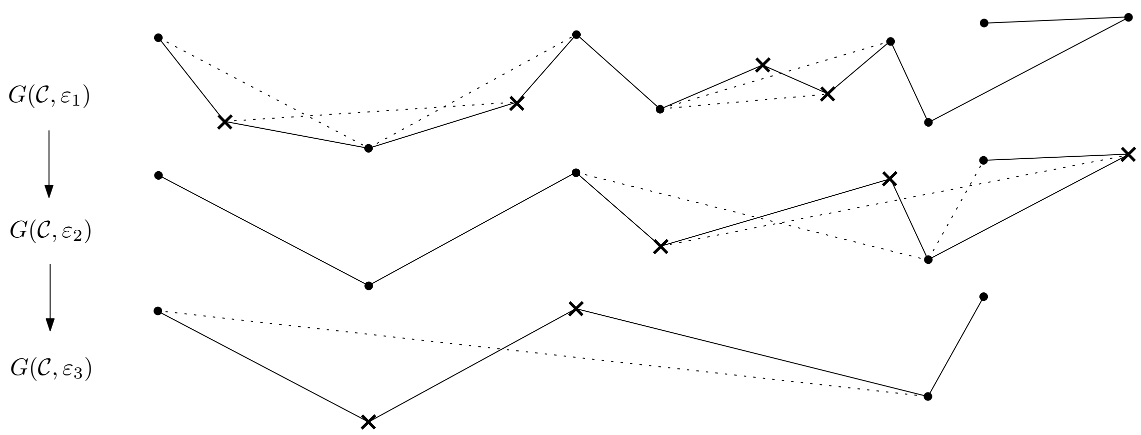
$G(\mathcal{C}, \varepsilon_1)$
$G(\mathcal{C}, \varepsilon_2)$
$G(\mathcal{C}, \varepsilon_3)$

Figure 5.4: Bottom-up greedy construction of progressive simplifications using Imai-Iri [16].

Optimization As for the top-down approach, we can improve the performance of this algorithm by integrating the construction of the shortcut graphs with the greedy choices that are made at every scale. Instead of pruning the shortcut graph on line 6, we can limit the search space while constructing the shortcut graph using ChinChan (see Section 4.1).

Consider we are constructing $G(\mathcal{C}, \varepsilon_k)$ for some $1 \leq k \leq m$. During the forward traversal of $\mathcal{C}$, we skip from p_i to p_{i+1} whenever $p_i \notin \mathcal{S}_{k-1}$. Furthermore, for every shortcut (p_i, p_j) where $p_j \notin \mathcal{S}_{k-1}$, we do not check whether p_j is inside the wedge w, since (p_i, p_j) cannot be included in $\mathcal{S}_k$. Note that we do intersect wedge w with wedge w_j, since there may be valid shortcuts (p_i, p_k) where $k > j$. Similar pruning is performed during the reverse traversal of $\mathcal{C}$.

Naive construction Cao et al. [5] devised an efficient heuristic for simplifying polygonal curves progressively. This heuristic works by constructing the shortcut graph at any scale $k > 1$ on $\mathcal{S}_{k-1}$, instead of on $\mathcal{C}$. This way, we can obtain $\mathcal{S}_k$ by finding a shortest path from p_1 to p_n in $G(\mathcal{S}_{k-1}, \varepsilon_k)$, as opposed to the pruned shortcut graph $G(\mathcal{C}, \varepsilon_k)$. Although this would improve the running time since $|\mathcal{S}_{k-1}| \leq |\mathcal{C}|$, guarantees on the maximum error are lost. This is illustrated for the Hausdorff distance in Figure 5.5. Note how for higher scales, the simplifications become progressively worse in terms of the Hausdorff distance to the input curve. The bound on the error of simplification $\mathcal{S}_k$ is $\max_{(p_i,p_j)\in\mathcal{S}_k} \mathcal{H}(\langle p_i, \dots, p_j\rangle, \langle p_i, p_j\rangle) \leq \sum_{\ell=1}^{k} \varepsilon_\ell$ for all $1 \leq k \leq m$.

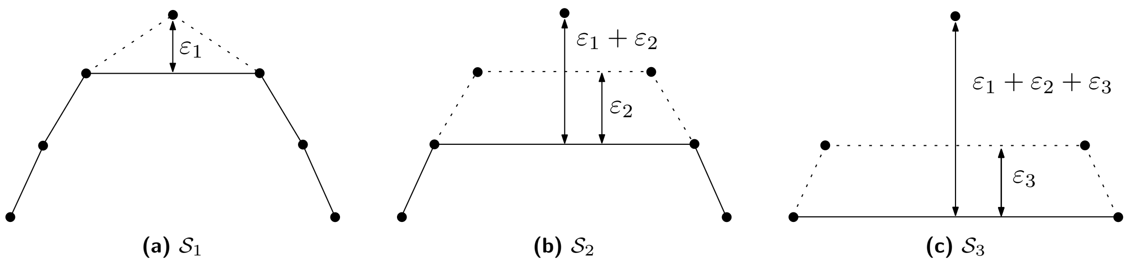

Figure 5.5: Naive bottom-up construction of simplifications using shortcut graphs. The Hausdorff distance to the input curve becomes progressively larger.

5.2.3 Integrating Single-Scale Simplification

The structure of ImaiIriTopDown (Algorithm 5.2) can trivially be exploited to facilitate other simplification techniques. We do this by replacing the shortest path queries with any algorithm that solves Single Scale Min-# either optimally or greedily.

Such an algorithm was developed by Ramer [20], and Douglas and Peucker [10], which greedily simplifies polygonal curves under the Hausdorff distance. For any polygonal curve $\mathcal{C} = \langle p_1, \dots, p_n \rangle$, this algorithm recursively splits the polygonal curve in two until the remaining subcurves can safely be replaced with a single line segment. The splitting point p_s is found for any subcurve $\mathcal{C}' = \langle p_i, \dots, p_j \rangle \sqsubseteq \mathcal{C}$ by finding the furthest point in $\mathcal{C}'$ from the line segment (p_i, p_j). Pseudo code for this simplification heuristic is given in Algorithm 5.4.

Algorithm 5.4 DouglasPeucker($\mathcal{C}, \varepsilon$)

```
1:  $d_{max} \leftarrow 0$
2:  for $i \leftarrow 2$ to $n-1$ do
3:      $d_i \leftarrow dist(p_i, (p_1, p_n))$
4:      if $d_i > d_{max}$ then
5:          $d_{max} \leftarrow d_i$
6:          $p_s \leftarrow p_i$
7:      end if
8:  end for
9:  if $d_{max} > \varepsilon$ then
10:     $\mathcal{S}_1 \leftarrow$DouglasPeucker($p_1, \dots, p_s$, $\varepsilon$)
11:     $\mathcal{S}_2 \leftarrow$DouglasPeucker($p_s, \dots, p_n$, $\varepsilon$)
12:     $\mathcal{S} \leftarrow \mathcal{S}_1 \cup \mathcal{S}_2$                    Include $p_s$ only once
13: else
14:     $\mathcal{S} \leftarrow \langle p_1, p_n \rangle$
15: end if
16: return $\mathcal{S}$
```

The simplification heuristic by Cao et al. [5] discussed in Section 5.2.2 works for any curve simplification algorithm, and can therefore be applied to DouglasPeucker. We thus have $\mathcal{S}_k =$ DouglasPeucker$(\mathcal{S}_{k-1}, \varepsilon_k)$ for any $1 < k \leq m$. Despite this naive construction heuristic, we retain our bound on the Hausdorff distance across all scales, since the algorithm splits each subcurve on the furthest point from the corresponding shortcut. This is unlike the naive bottom-up construction using shortcut graphs as discussed in Section 5.2.2. Furthermore, as a result of this splitting strategy, constructing from the bottom up always yields the same simplification as constructing from the top down.

Running time If we expect that every split of every subcurve $\mathcal{C}' \sqsubseteq \mathcal{C}$ is roughly in the middle, the expected running time complexity of this algorithm can be described by the linear recurrence $T(n) = 2T(\frac{n}{2}) + O(n)$. Solving this recurrence using the Master theorem yields $T(n) \in \Theta(n \log n)$ meaning the expected running time of DouglasPeucker to greedily solve Single Scale Min-# is $\Theta(n \log n)$. In the worst case, every split yields a subcurve with size $\Theta(n)$, meaning that the worst-case running time is $\Theta(n^2)$.

We conclude that both the top-down and the bottom-up extension of DouglasPeucker to greedily solve Progressive Min-# yields an expected running time of $\Theta(nm \log n)$, and a worst case running time of $\Theta(n^2 m)$.

5.2.4 Worst-case Performance

One disadvantage of using greedy algorithms for progressive curve simplifications is that a single bad choice on a certain scale can lead to a poor simplification on another scale. To highlight this, consider Figure 5.6. Here we see a recurring zigzag pattern of points between p_i and p_j with a length of $O(n)$. Note that the subcurve $\langle p_i, \dots, p_j \rangle$ can only be simplified by $\langle p_i, p_j \rangle$ for any error bound $\varepsilon \geq \varepsilon_x$. Therefore, any greedy choice that excludes $\langle p_i, p_j \rangle$ yields a simplification that is $O(n)$ larger than the minimum.

Consider the case where $\varepsilon_1 = \varepsilon_x$ and $\varepsilon_2 = \varepsilon_y$. In this case, ImaiIriBottomUp includes shortcut $(p_i, p_j) \in \mathcal{S}_1$. However, ImaiIriTopDown yields a simplification $\mathcal{S}_2 = \langle p_1, p_{i+1}, p_n \rangle$ using ε_y at the second scale. This results in an independent simplification of $\langle p_1, \ldots, p_{i+1} \rangle$ and $\langle p_{i+1}, \ldots, p_n \rangle$ at the first scale using ε_x. Therefore, shortcut (p_i, p_j) cannot be included in $\mathcal{S}_1$, meaning ImaiIriTopDown is forced to include $\langle p_{i+1}, \ldots, p_j \rangle$ in $\mathcal{S}_1$.

Next, consider the case where $\varepsilon_1 = 0$ and $\varepsilon_2 = \varepsilon_x$. ImaiIriTopDown will efficiently simplify $\langle p_i, \ldots, p_j \rangle$ at the second and first scale. However, ImaiIriBottomUp removes p_i using $\varepsilon_1 = 0$ since it lies on the line segment (p_1, p_{i+1}). This however removes the possibility of including shortcut (p_i, p_j) at the second scale. ImaiIriBottomUp thus must include $\langle p_{i+1}, \ldots, p_j \rangle$ in $\mathcal{S}_2$.

Note that in both cases, both a bottom-up and top-down construction of a progressive simplification using DouglasPeucker will fail to include (p_i, p_j) in any simplification, due to its splitting heuristic.

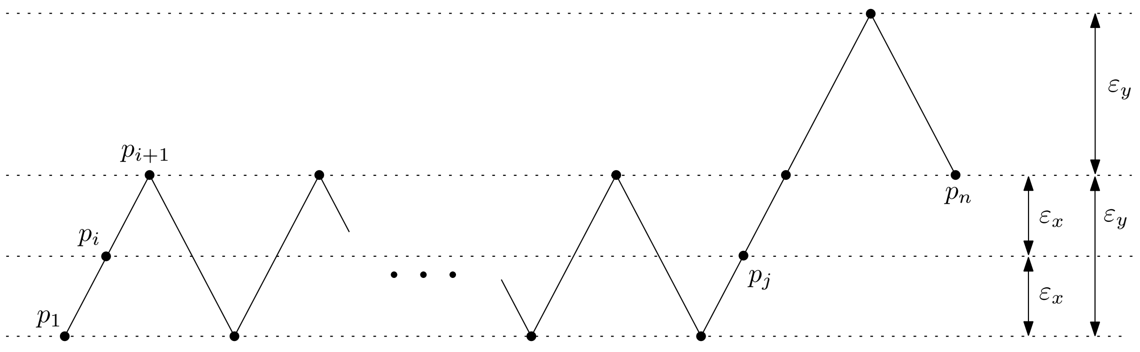

Figure 5.6: Problematic case for the greedy construction algorithms.

5.3 Experimental Evaluation

We explore how the real-world performance of every proposed progressive simplification algorithm relates to its theoretical asymptotic running time. We therefore experimentally investigate the performance of each simplification algorithm along two dimensions: the length of the input curve, and the number of scales.

For the experimental setup, refer to Section 3.3.

5.3.1 Performance by Curve Length

To gain general insights into the performance of every simplification algorithm – both in terms of running time and simplification complexity – we experimentally evaluate how the performance of each algorithm relates to the length of the input curve. For these experiments, we fix the number of scales to 10. Furthermore, we linearly sample the error bounds from the smallest shortcut error up to the tenth shortcut error percentile, yielding a density of 10% for shortcut graph $G(\mathcal{C}, \varepsilon_m)$. For every algorithm, we measure both its running time, and the cumulative simplification size $\sum_{i=1}^{m} |\mathcal{S}_i|$.

To gauge how the running time is influenced by imposing monotonic containment on the simplifications, we use a non-progressive simplification algorithm (II Non Prog.), which independently constructs min-# simplifications using shortcut graphs (See Section 2.3).

All shortcut graphs are represented using shortcut interval sets constructed by ChinChan (Algorithm 4.1), on which we compute shortest paths using range queries (Section 3.2). As discussed in Section 5.1.1, we cannot use shortcut interval sets for ImaiIriProgressive. However, we do wish to efficiently detect all shortcuts by using shortcut intervals in conjunction with ChinChan. Therefore, this algorithm is implemented such that ChinChan provides the algorithm with shortcut interval sets, from which every shortcut is copied to an explicit shortcut graph. On each such shortcut graph, we then compute shortest paths with an implementation of Dijkstra's algorithm [9] using a priority queue implemented by a pairing heap [11]. This is a popular and flexible heap type commonly used for Dijkstra's algorithm. Testing shows that for finding shortest paths in shortcut graphs, pairing heaps show similar or better performance compared to other popular heap types such as d-ary heaps, Fibonacci heaps, or binomial heaps.

The running time and cumulative simplification size of each algorithm for various lengths of the input curve is given in Table 5.1. Plotting these running times yields Figure 5.7. ImaiIriProgressive (II Prog.) exhibits running times that are at least an order of magnitude worse than every other algorithm. The performance of ImaiIriTopDown (II TD) is worse than ImaiIriBottomUp (II BU) since it performs less pruning in the search space of each shortcut graph.

	Length of the input curve									
	500		1500		2500		3500		5000	
	sec.	#	sec.	#	sec.	#	sec.	#	sec.	#
II Prog.	0.651	719	7.258	636	24.269	640	52.740	596	146.64	647
II Non Prog.	0.290	646	2.357	570	6.187	568	10.921	520	21.454	576
II TD	0.242	1066	1.915	1277	4.542	1455	8.177	1432	16.328	1600
II BU	0.076	814	0.278	723	0.618	733	0.989	680	1.645	717
II BU Cao	0.026	751	0.097	675	0.215	690	0.402	624	0.784	655
DP TD	0.0039	849	0.0111	862	0.017	879	0.025	885	0.039	1010
DP BU	0.0046	849	0.0091	862	0.012	879	0.016	885	0.023	1010

Table 5.1: Running time in seconds and cumulative simplification size for various lengths of the input curve and 10 scales.

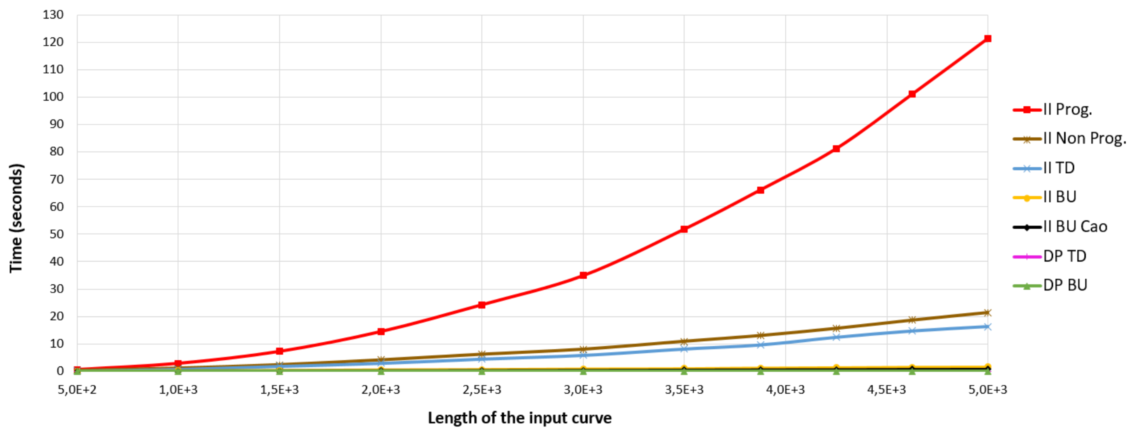

Figure 5.7: Running time for various lengths of the input curve and 10 scales.

To evaluate the running time of the other algorithms, consider Figure 5.8. We observe that naive bottom-up construction as presented in Section 5.2.2 (II BU Cao) is consistently twice as fast as II BU. Furthermore, both the top-down construction (DP TD) and bottom-up construction (DP BU) using DouglasPeucker run in linear time in the length of the input curve, and are an order of magnitude faster than the other greedy algorithms. DP BU exhibits running times that are around 40% faster than DP TD. For few points, DP TD is faster than DP BU due to the benefits of the divide-and-conquer approach of DP TD, which for small input curves outweighs the time saved by DP BU's pruning of the shortcut graphs.

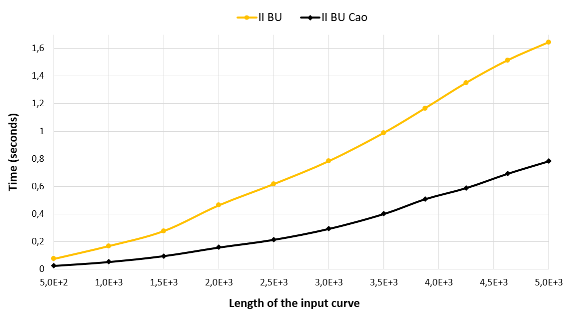

(a) II BU and II BU Cao

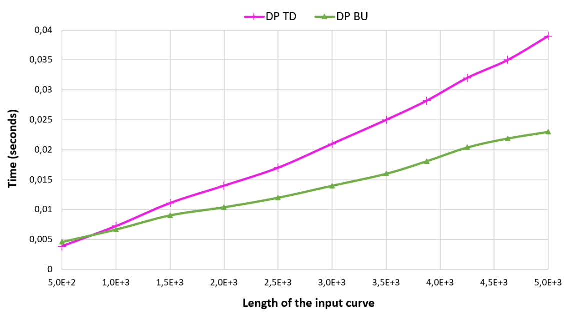

(b) DP TD and DP BU

Figure 5.8: Running time of the greedy algorithms for various lengths of the input curve and 10 scales.

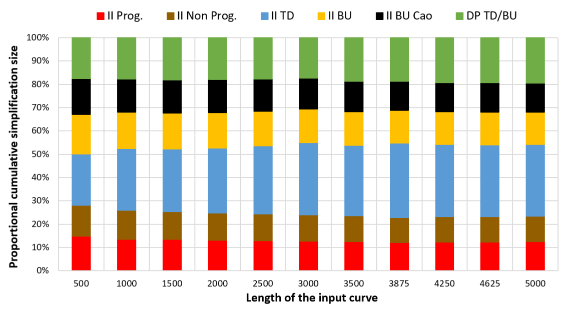

(a) Proportions by length of the input curve

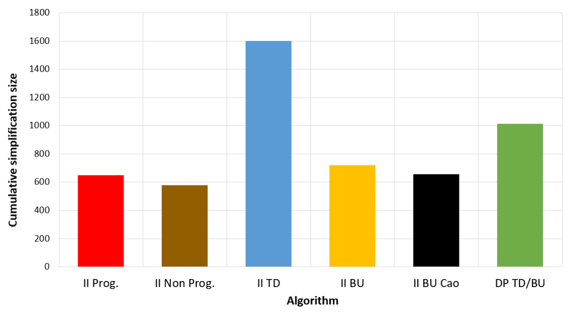

(b) 5000 points

Figure 5.9: Cumulative simplification size for 10 scales.

Aside from the running time, we are interested in the cumulative size of the progressive simplifications produced by the algorithms. In Figure 5.9a, we see how these cumulative simplification sizes relate proportionally. We observe that for large curves, II TD produces simplifications that are proportionally larger when compared to smaller input curves. This is explained by the greedy choice strategy of II TD, which starts with a greedy choice on $\mathcal{S}_m$. Any error made in this simplification propagates to all lower scales. Therefore, II TD starts with the most aggressive greedy choice. The extent of a poor greedy choice for $\mathcal{S}_m$ exacerbates for larger input curves.

The proportions however do stabilize for larger input curves. A visualization of the cumulative simplification size of each algorithm for the largest input curve (5000 points) is given in Figure 5.9b. Note that II Prog. yields the best progressive simplification, which is 12% larger than the best possible non-progressive simplification obtained by II Non Prog. The second best progressive simplification is produced by II BU, which is 11% larger than II Prog. This simplification size is further lowered by II BU Cao, which does so by relaxing the error bound. This algorithm produces a simplification that is 8.5% smaller than II BU, and 1.2% larger than II Prog.

Next, let us investigate how the cumulative simplification size is distributed over all scales for each algorithm. For this, we use the same parameters, but simplify for 15 scales instead of 10. The results are listed in Table 5.2, and plotted on a logarithmic scale in Figure 5.10.

Despite starting at the highest scale, II TD produces a simplification at scale 14 that is worse compared to the other algorithms. Furthermore, note that despite its poor cumulative simplification size, II TD does produce the best simplification for the highest scale.

	Simplification size														
	1	2	3	4	5	6	7	8	9	10	11	12	13	14	15
II Prog.	412	149	118	89	75	64	50	45	38	32	31	29	25	25	24
II Non Prog.	402	136	95	73	59	51	37	35	32	29	27	25	24	22	20
II TD	812	519	395	314	255	214	179	150	122	101	82	66	51	35	20
II BU	402	203	146	106	87	66	59	47	44	38	35	33	31	29	28
II BU Cao	402	168	123	99	76	67	53	45	41	36	33	29	29	29	25
DP TD/BU	553	287	184	126	97	73	62	51	47	44	40	40	36	33	32

Table 5.2: Simplification size at every scale for 5000 points and 15 scales.

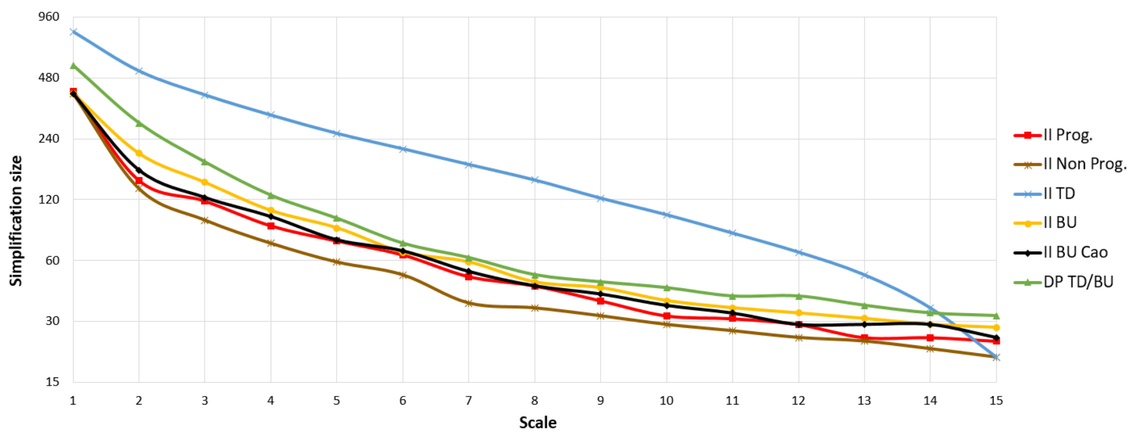

Figure 5.10: Simplification size at every scale on a logarithmic scale, for 5000 points and 15 scales.

We conclude that in practice, ImaiIriProgressive yields simplifications that are comparable in size to minimal non-progressive simplifications. However, it is too slow to be used on larger input curve. This makes ImaiIriBottomUp a sensible alternative which is significantly faster and yields simplifications that are only slightly larger. New techniques for finding shortest paths on weighted shortcut graphs have to be developed to improve the scalability of ImaiIriProgressive.

Furthermore, top-down construction by ImaiIriTopDown was shown to be significantly worse than ImaiIriBottomUp, both in terms of running time and simplification complexity.

Finally, bottom-up construction of progressive simplifications using the well known algorithm by Douglas and Peucker [10] yields the best running-time performance in practice for all lengths of the input curve, and is thus the most scalable progressive simplification algorithm. However, it generates simplifications that are up to 56% larger than simplifications produced by ImaiIri-Progressive, which is unsuitable in settings where the cumulative complexity of the progressive simplification is critical.

5.3.2 Performance by Number of Scales

We investigate how the running time and cumulative simplification size relates to the number of scales. For these experiments, we fix the length of the input curve to 3000 points. The results are given in Table 5.3. Note that for a single scale, every algorithm produces an optimal simplification, except for the heuristic-based algorithms DP TD and DP BU.

A plot of the running times is given in Figure 5.11. Note the linear relation between the running time and the number of scales. We observe a growth in running time of II Prog. that is around four times that of II Non Prog.

	Number of scales									
	1		8		20		44		68	
	sec.	#	sec.	#	sec.	#	sec.	#	sec.	#
II Prog.	3.056	20	29.143	435	68.743	1573	133.40	4297	197.01	7331
II Non Prog.	1.992	20	6.588	384	14.772	1397	32.265	3719	47.796	6356
II TD	1.986	20	4.889	1020	8.557	4643	16.254	13191	23.574	22198
II BU	1.995	20	0.749	509	1.188	1822	2.459	4958	3.708	8356
II BU Cao	1.993	20	0.351	467	0.209	1696	0.202	4599	0.244	7825
DP TD	0.0070	29	0.018	649	0.033	2119	0.060	5443	0.088	9013
DP BU	0.0068	29	0.016	649	0.019	2119	0.33	5443	0.047	9013

Table 5.3: Running time in seconds and cumulative simplification size on 3000 points for various numbers of scales.

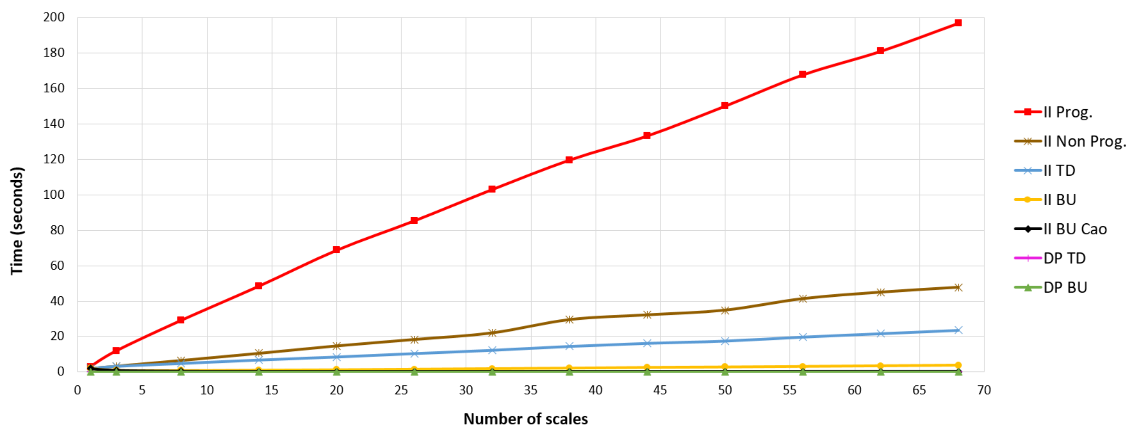

Figure 5.11: Running time on 3000 points for various numbers of scales.

The running times of the other algorithms are visualized in Figure 5.12. Unlike all other algorithms, II BU Cao is faster for many scales, which is related to the sampling of error bounds. By sampling more error bounds, the first error bound ε_1 becomes smaller, which means the construction of shortcut graph $G(\mathcal{C}, \varepsilon_1)$ using ChinChan (Algorithm 4.1) is faster, due to the additional pruning. II BU Cao prunes drastically at the first scale, and thus its running time is almost fully determined by the time spent on the first simplification.

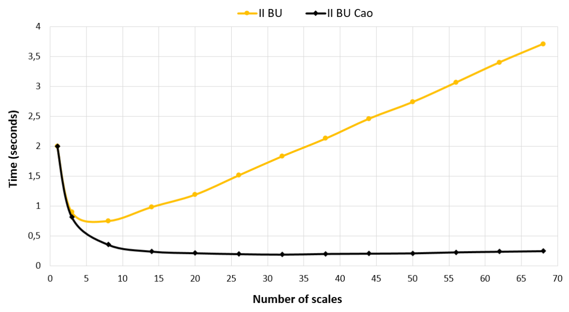

(a) II BU and II BU Cao

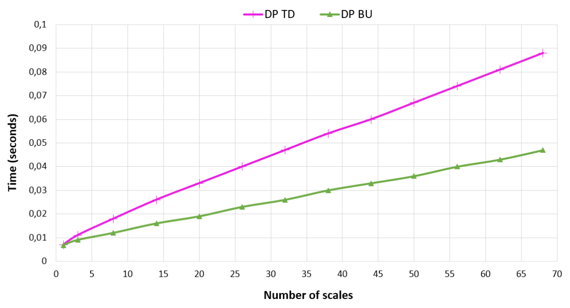

(b) DP TD and DP BU

Figure 5.12: Running time of the greedy algorithms on 3000 points for various numbers of scales.

Recall that II BU performs less pruning, since shortcuts in $\mathcal{S}_k$ are detected in $\mathcal{C}$ instead of $\mathcal{S}_{k-1}$. II BU performs best around 7 scales, where there is significant pruning at the first scale without spending too much time constructing simplifications at higher scales.

We observe that DP BU is 45% more efficient than DP TD. The growth in running time for both algorithms in the number of scales is much like the growth in the length of the input curve observed in Figure 5.8b.

Finally, consider Figure 5.13, where the the cumulative simplification sizes are visualized for various numbers of scales. In Figure 5.13a, we observe the relative cumulative simplification size given by II TD increases for many scales, since poor greedy choices at higher scales cascade across more scales. Furthermore, we observe that the relative cumulative simplification size of DP TD/BU decreases as the number of scales grows. A visualization of the cumulative simplification size of each algorithm for 68 scales is shown in Figure 5.13b.

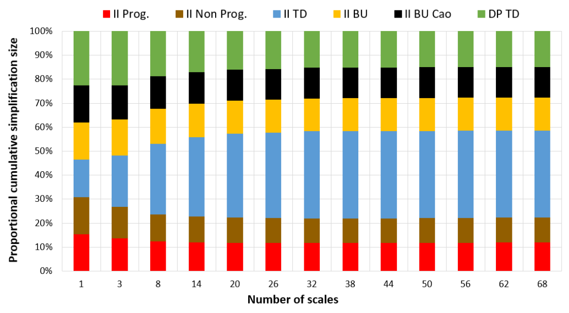

(a) Proportions by number of scales

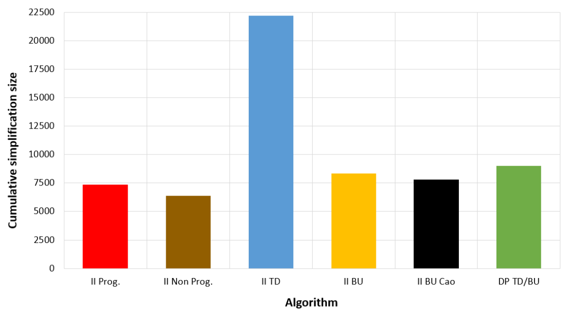

(b) 68 scales

Figure 5.13: Cumulative simplification size on 3000 points.

In conclusion, all algorithms exhibit performance linear in the number of scales, except II BU Cao, which performs best on many scales. The same trade-offs exist between running time and simplification size as described in Section 5.3.1. The most notable difference is that for many scales, DP TD and DP BU yield a relative simplification size that is better than for fewer scales. Thus, DP BU is a reasonable alternative to II Prog. when simplifying for many different levels of detail.

Chapter 6

Conclusions and Future Work

In this thesis we investigated both the theoretical and practical aspects of progressive simplification of polygonal curves. Progressive simplification enables exploration of zoomable visualizations of spatial data by imposing consistency between simplifications at different levels of detail. We aimed to bridge the gap between existing heuristic-based algorithms for producing progressive simplifications, and minimum-link non-progressive simplification algorithms. To solve this problem, we developed multiple extensions for a common non-progressive minimum-link simplification algorithm [16] using so-called shortcut graphs.

We developed an optimal algorithm that runs in $O(n^3m)$ time, and produces simplifications by finding shortest paths in *weighted* shortcut graphs where the weight of an edge (p_i, p_j) at scale k encodes the cost of the best possible sequence of simplifications up to scale k on the subcurve from p_i to p_j.

We further developed two greedy progressive simplification algorithms with a running time of $O(n^2m)$. These algorithms construct the simplifications in a certain order (bottom-up or top-down), while enforcing monotonic containment. Because each simplification is constructed using local minima, these algorithms do not strictly minimize the combined simplification complexity.

To efficiently construct shortcut graphs for multiple different error bounds, we developed an algorithm that determines the Hausdorff distance [12] of every shortcut to the associated contiguous subsequence on the input curve. This allows us to efficiently determine shortcut validity for any error bound. The algorithm runs in $O(n^2 \log n)$ time, which is an improvement over $O(n^3)$ time using existing techniques [16]. Experimental evaluation reveals that this algorithm is only viable for a large number of scales, compared to independent construction of each shortcut graph for a fixed error bound using existing algorithms [6]. This makes it a good choice for computing continuous progressive simplifications in $O(n^5)$ time using $\binom{n}{2}$ scales.

To quickly find shortest paths in unweighted shortcut graphs, we developed a representation of the shortcut graph called a *shortcut interval set*. This representation was shown to be of linear size in practice, which allows for finding shortest paths in $O(n \log n)$ time, yielding near-linear performance in practice. This is a significant improvement over the quadratic running-time performance given by breadth-first search. Furthermore, we showed how construction of shortcut interval sets can be integrated with existing techniques [6] to significantly speed up construction of shortcut graphs under the Hausdorff distance in practice. Shortcut interval sets can thus be integrated with all aspects of min-# curve simplification using shortcut graphs, lowering the storage requirements from $O(n^2)$ to $O(n)$. This greatly improves the scalability of using shortcut graphs, both in progressive and non-progressive settings.

Experimental evaluation of the optimal progressive simplification algorithm reveals that it is not scalable to large input curves. We found that the best alternative is a bottom-up greedy construction of the simplifications using shortcut graphs, from the smallest error bound to the largest error bound. This greedy algorithm has excellent running-time performance in practice, while producing near-minimal progressive simplifications.

In conclusion, we have developed several progressive simplification algorithms where for each algorithm there exists a trade-off between scalability and simplification complexity. As a by-product of our endeavors, a space-efficient representation of the shortcut graph was developed which is not only applicable to progressive simplification, but also highly suitable for computing simplifications for a single error bound.

Although shortcut interval sets yield great benefits in practice, simplification for a single error bound takes quadratic time in practice to detect all shortcuts. As a future work, it might be of interest to further optimize the construction of shortcut interval sets. This could be a stepping stone towards the first near-linear min-# simplification algorithm. This is valuable, since existing high-performance simplification algorithms either heuristically aim for the smallest number of points [10], or approximate the minimum number points by a certain factor [1], and may thus produce simplifications which are significantly worse than the optimum.

We focused on the Hausdorff distance as error measure, though any error measure can be used to determine the validity of a shortcut. To efficiently employ the developed progressive simplification algorithms in other settings, it is of interest to develop efficient techniques for constructing shortcut graphs for error measures other than the Hausdorff distance, such as Fréchet [4] or area-based measures [8].

Bibliography

[1] Pankaj K. Agarwal, Sariel Har-Peled, Nabil H. Mustafa, and Yusu Wang. Near-linear time approximation algorithms for curve simplification. *Algorithmica*, 42(3–4):203–219, 2005. 2, 46

[2] Pankaj K. Agarwal and Kasturi R. Varadarajan. Efficient algorithms for approximating polygonal chains. *DCG*, 23(2):273–291, 2000. 2

[3] Sander Alewijnse, Kevin Buchin, Maike Buchin, Andrea Kölzsch, Helmut Kruckenberg, and Michel A Westenberg. A framework for trajectory segmentation by stable criteria. In *Proc. 22nd ACM SIGSPATIAL Internat. Conf. Advances in Geographic Information Systems*, pages 351–360. ACM, 2014. 10

[4] Helmut Alt and Michael Godau. Computing the Fréchet distance between two polygonal curves. *IJCGA*, 5(1–2):78–99, 1995. 1, 3, 46

[5] Hu Cao, Ouri Wolfson, and Goce Trajcevski. Spatio-temporal data reduction with deterministic error bounds. *VLDB J*, 15(3):211–228, 2006. 1, 37, 38

[6] Wing Shiu Chan and F Chin. Approximation of polygonal curves with minimum number of line segments or minimum error. *IJCGA*, 6(01):59–77, 1996. 2, 17, 18, 36, 45

[7] Thomas H. Cormen, Charles Eric Leiserson, Ronald L Rivest, and Clifford Stein. *Introduction to Algorithms*, chapter 13, pages 308–338. MIT press, 3rd edition, 2009. 13

[8] Shervin Daneshpajouh, Mohammad Ghodsi, and Alireza Zarei. Computing polygonal path simplification under area measures. *Graphical Models*, 74(5):283–289, 2012. 2, 4, 46

[9] Edsger W Dijkstra. A note on two problems in connexion with graphs. *Numerische mathematik*, 1(1):269–271, 1959. 32, 40

[10] David H Douglas and Thomas K Peucker. Algorithms for the reduction of the number of points required to represent a digitized line or its caricature. *Cartographica: The International Journal for Geographic Information and Geovisualization*, 10(2):112–122, 1973. 1, 2, 38, 42, 46

[11] Michael L Fredman, Robert Sedgewick, Daniel D Sleator, and Robert E Tarjan. The pairing heap: A new form of self-adjusting heap. *Algorithmica*, 1(1):111–129, 1986. 40

[12] Felix Hausdorff. *Grundzüge der Mengenlehre.* Verlag Von Veit & Comp., 1914. 1, 3, 45

[13] John Hershberger and Jack Snoeyink. An $O(n \log n)$ implementation of the Douglas-Peucker algorithm for line simplification. In *Proc. 10th Sympos. Comp. Geom.*, pages 383–384. ACM, 1994. 2

[14] John Hershberger and Jack Snoeyink. Cartographic line simplification and polygon csg formulae in $O(n \log^* n)$ time. *Computational Geometry*, 11(3-4):175–185, 1998. 2

[15] Hiroshi Imai and Masao Iri. Computational-geometric methods for polygonal approximations of a curve. *Comput. Vis. Graph. Image Process.*, 36(1):31–41, 1986. 2

[16] Hiroshi Imai and Masao Iri. Polygonal approximations of a curve – formulations and algorithms. In G. T. Toussaint, editor, *Computational Morphology*, pages 71–86. Elsevier, 1988. 2, 7, 8, 17, 19, 27, 37, 45

[17] Avraham Melkman and Joseph O'Rourke. On polygonal chain approximation. In G. T. Toussaint, editor, *Computational Morphology*, pages 87–95. Elsevier, 1988. 2

[18] Edward F Moore. The shortest path through a maze. In *Proc. International Symposium on the Theory of Switching*, pages 285–292. Harvard University Press, 1959. 7, 10

[19] Guo Qingsheng, Christoph Brandenberger, and Lorenz Hurni. A progressive line simplification algorithm. *Geo-spatial Information Science*, 5(3):41–45, 2002. 2

[20] Urs Ramer. An iterative procedure for the polygonal approximation of plane curves. *Computer graphics and image processing*, 1(3):244–256, 1972. 38

[21] Daniel Schmidt-Rothmund. Griffon Vulture NABU Moessingen, 186178781. *Movebank: archive, analysis and sharing of animal movement data. World Wide Web electronic publication*, `http://www.movebank.org` accessed in June 2017. 12

[22] Robert Sedgewick. Left-leaning red-black trees. In *Dagstuhl Workshop on Data Structures*, page 17, 2008. 13, 27

[23] G. T. Toussaint. On the complexity of approximating polygonal curves in the plane. In *Proc. IASTED, Internat. Sympos. Robotics and Automation*, 1985. 2

[24] Maheswari Visvalingam and James D Whyatt. Line generalisation by repeated elimination of points. *Cartogr J*, 30(1):46–51, 1993. 1, 2